Dual-UAV Enabled Secure Data Collection With Propulsion Limitation

Ran Zhang, Xiaowei Pang, Weidang Lu, *Member, IEEE,* Nan Zhao, *Senior Member, IEEE,* Yunfei Chen, *Senior Member, IEEE,* and Dusit Niyato, *Fellow, IEEE*

***Abstract*—Unmanned aerial vehicles (UAVs) have been widely utilized to improve the end-to-end performance of wireless communications. However, its line-of-sight makes UAV communication vulnerable to malicious eavesdroppers. In this paper, we propose two cooperative dual-UAV enabled secure data collection schemes to ensure security, with the practical propulsion energy consumption considered. We first maximize the worst-case average secrecy rate with the average propulsion power limitation, where the scheduling, the transmit power, the trajectory and the velocity of the two UAVs are jointly optimized. To solve the non-convex multivariable problem, we propose an iterative algorithm based on block coordinate descent and successive convex approximation. To further save the on-board energy and prolong the flight time, we then maximize the secrecy energy efficiency of UAV data collection, which is a fractional and mixed integer nonlinear programming problem. Based on the Dinkelbach method, we transform the objective function into an integral expression and propose an iterative algorithm to obtain a suboptimal solution to secrecy energy efficiency maximization. Numerical results show that the average secrecy rate is maximized in the first scheme with propulsion limitation, while in the second scheme, the secrecy energy efficiency is maximized with the optimal velocity to save propulsion power and improve secrecy rate simultaneously.**

***Index Terms*—Cooperative jamming, data collection, physical layer security, power allocation, secrecy energy efficiency, unmanned aerial vehicle.**

I. Introduction

Unmanned aerial vehicles (UAVs) can be controlled remotely by a pilot, or be preprogrammed to fly autonomously. Over the past decade, UAVs have been used in areas ranging from agriculture to industry or simply as a hobby [2]. Due to the advantages, such as low cost and high mobility, UAVs are envisioned to play an important role in future wireless networks, and provide seamless and ubiquitous wireless connectivity [3]. Two typical scenarios of UAV-assisted communications are emergency communication and long-distance relay. The terrestrial data transmission will suffer from outage when emergencies occur, and UAVs can be deployed as temporary aerial base stations (BSs) to deliver broadband wireless connectivity in hot-spot areas in [4], [5]. Furthermore, UAV relay can be applied as a "communication bridge" to support reliable connectivity from source to destination [6], [7].

The deployment and dynamic movement of UAV is a unique characteristic for UAV-assisted communications. In order to address the issue of UAV deployment, Al-Hourani *et al.* in [8] derived the optimal altitude of a static UAV to provide a maximum coverage radius. Based on [8], Mozaffari *et al.* considered multiple re-transmissions for the UAV and device-to-device (D2D) users in [9], where the overall coverage probability of the D2D users was derived. In [10], a novel three-dimensional system model and an analytical framework were proposed by Lyu and Zhang to characterize the coverage performance of UAV. Furthermore, the optimization of UAV trajectory has drawn significant interest recently. In [11], Lyu *et al.* maximized the minimum average rate among the users with the UAV flying in a straight line. Wu *et al.* extended the results of [11] to the case of multiple UAVs in [12] to optimize the trajectories and resource allocation. In [13], UAV-enabled interference channel was studied by Shen *et al.* to address the strong cross-link interference issue.

The propulsion power of UAV is mainly provided by batteries, but their long charging time and low energy density make the UAV unable to keep flying. However, increasing the number of batteries is not a practical solution due to weight and space constraints. It is worth to mention that flight endurance can be improved by UAV trajectory optimization to affect the propulsion power consumption via velocity. To this end, the theoretical closed-form expressions of propulsion energy consumption models for rotary-wing and fixed-wing UAVs were derived by Zeng *et al.* in [14] and [15], respectively. Based on the mathematical model for rotary-wing UAVs, Zhan and Lai minimized the UAV energy consumption for the Internet of Things (IoT) systems [16], and Zhang *et al.* focused on the energy efficiency of UAV in a mobile edge computing system [17]. With the aid of non-orthogonal multiple access (NOMA), Pang *et al.* studied the energy-efficient resource allocation for mmWave-enabled UAV networks [18]. Turgut *et al.* presented a novel framework in [19], for analyzing the energy coverage performance of UAV energy harvesting networks. In addition, the maximization of energy efficiency

were investigated for fixed-wing UAVs in [20]–[22]. In some scenarios, we need to collect data and analyze the status of ground sensor nodes (SNs). Utilizing UAV as a data collector is an energy-efficient method to complete this task, because UAV can take full advantage of its mobility to schedule the SNs sequentially, and each SN can directly transmit its information to the UAV [23]. Zhan *et al.* minimized the maximum energy consumption of all the SNs when a UAV collector was used to gather information [24]. This work was then extended in [25] by studying the fundamental tradeoff between the aerial and ground cost.

Although UAVs can provide a high probability to establish strong line-of-sight (LoS) air-to-ground channels, it also increases the risk of being eavesdropped [26]. Different from traditional methods to enhance the security in terrestrial communication systems, UAV can utilize its high mobility and flexibility to avoid being eavesdropped via adjusting its flight trajectory. For instance, the UAV can fly close to the legitimate user or fly away from the eavesdropper via trajectory optimization, and thus the average secrecy rate can be improved in the presence of a single eavesdropper [27], multiple eavesdroppers [28], or eavesdroppers with unknown locations [29]. Furthermore, adding artificial noise was an effective method to further improve the security of the UAV communication [30]–[34]. Li *et al.* proposed a mobile UAV jamming scheme in [30], where the UAV can transmit jamming signals to fight against eavesdropping. In [31], Cai *et al.* considered a dual-UAV system with the assistance of a jamming UAV. Based on the dual-UAV model, a simultaneous wireless information and power transfer (SWIPT) enabled receiver was considered by Mamaghani and Hong for security and energy scavenging [32]. Wang *et al.* [33] considered the SWIPT when artificial jamming was generated to guarantee the secure NOMA transmission. Then, Mamaghani and Hong proposed a novel two-phase transmission protocol in UAV secure communication to enhance the ASR performance [34]. Recently, reinforcement learning has been developed to address the optimization for communications, e.g., the trajectory design for full-duplex UAV secure relaying in [35]. A multi-antenna jamming UAV was studied by Cai *et al.* in [36] to mitigate the interference upon legitimate users. The UAV can be also applied as a mobile relay to guarantee the network security via jointly optimizing the resource and trajectory [37]. An energy-efficient computation offloading technique for UAV mobile edge computing systems was proposed by Bai *et al.* in [38] to prevent information leakage. Moreover, Hua *et al.* considered a downlink transmission system with fixed-wing UAVs, and proposed a novel scheme to improve the secrecy energy efficiency in the presence of multiple source UAVs and multiple jamming UAVs in [39].

In the scenario where the UAV is dispatched as a mobile data collector to gather information from fixed ground nodes, a potential eavesdropper on the ground may intercept and wiretap the transmission. In order to improve the security, the UAV can fly closer to the nodes to establish better legitimate channels, and the nodes can also reduce their uplink transmit power to weaken the wiretap channels. Meanwhile, another cooperative jamming UAV can fly closer to the eavesdropper to enhance the jamming channel. However, such movement usually requires more propulsion energy consumption, and the limited on-board energy will constrain the flight time of UAV. Thus, the trajectory and velocity should be properly controlled to save the UAV's energy. To the best of our knowledge, very few works have investigated the security of data collection for energy-efficient dual-UAV systems.

Motivated by this demand, in this paper, a novel model of dual-UAV enabled secure data collection communication is designed to ensure the security, by considering the propulsion energy consumption for practical design under the limited on-board energy. The main contributions of this paper can be summarized as follows.

- We propose a dual-UAV cooperative jamming model for data collection, where a legitimate UAV receiver aims at collecting confidential data from ground nodes in the presence of a potential eavesdropper. To combat the eavesdropping, another cooperative UAV acts as a mobile jammer to disrupt the eavesdropping by sending artificial noise. In this dual-UAV network, the scheduling, the transmit power, and the trajectory and velocity of the two UAVs are optimized to improve the performance.
- The worst-case sum average secrecy rate is maximized among ground nodes with the average propulsion power budget. Since the optimization problem is difficult to solve due to the non-convexity, we divide it into four subproblems, which are transformed into approximated convex forms via the successive convex approximation (SCA). Then, the block coordinate descent (BCD) is employed to address these subproblems successively.
- We consider the tradeoff between maximizing the total information bits and minimizing the total propulsion energy consumption. Thus, we formulate a second optimization problem to maximize the secrecy energy efficiency, which is a fractional and mixed integer nonlinear programming problem. Based on the Dinkelbach method, we transform the objective function into an integral expression, and propose an iterative algorithm to obtain a suboptimal solution.

The remainder of this work is organized as follows. In Section II, the system model is presented. Section III formulates the sum average secrecy rate maximization problem and proposes an iterative algorithm to solve it. Then, the secrecy energy efficiency is maximized in Section IV. Simulation results are demonstrated in Section V. Finally, Section VI concludes this paper.

II. System Model

Consider a dual-UAV enabled wireless network as in Fig. 1, where a legitimate UAV receiver (Bob) is working in a time division (TD) mode to collect confidential information from K ground nodes (Alice). A potential eavesdropper (Eve) endeavors to wiretap the legitimate transmission. In order to enhance the wireless security, another UAV (Jack) acts as a mobile jammer to disrupt the eavesdropping via artificial noise, and Alice has no prior knowledge of the noise-like interference

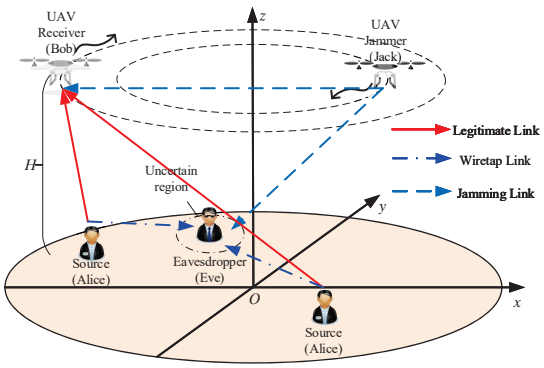

Fig. 1. Dual-UAV enabled secure communication system.

from Jack. We use subscripts or superscripts $\mathrm{A}, \mathrm{B}, \mathrm{J}$ and E to represent the terms associated with Alice, Bob, Jack and Eve, respectively. Assume that all the devices are equipped with a single antenna, and only partial information about the eavesdropper is available at the UAVs. In addition, we also assume that Eve has the perfect knowledge of all the CSI from Alice and Jack to herself, which is the worst case for Alice, but the best for Eve.

Without loss of generality, we consider a three-dimensional (3D) Cartesian coordinate system, where Bob and Jack fly at a fixed altitude H in meters and their horizonal coordinates are denoted by $\mathbf{q}_{\mathrm{B}}(t) = [x_{\mathrm{B}}(t), y_{\mathrm{B}}(t)]^T$ and $\mathbf{q}_{\mathrm{J}}(t) = [x_{\mathrm{J}}(t), y_{\mathrm{J}}(t)]^T$, $0 \le t \le T$, T is the flight duration. Then, the instantaneous velocity of Bob and Jack can be expressed as $\mathbf{v}_{\mathrm{B}}(t) \triangleq \mathbf{q}_{\mathrm{B}}^{'}(t)$ and $\mathbf{v}_{\mathrm{J}}(t) \triangleq \mathbf{q}_{\mathrm{J}}^{'}(t)$, respectively.

Trajectory discretization is adopted to divide the flight duration T into N time slots with the same time interval $\delta_t = T/N$, which is small enough to make the trajectory in each slot approximate to be a straight line. In each time slot, the channel state information can be also regarded as static due to the small δ_t. Assume that the legitimate channel and jamming channel can be approximated as line-of-sight (LoS) links[1], and the legitimate channel power from the kth Alice to Bob in the nth time slot follows the free-space path loss model as

$$g_{k\mathrm{B}}[n] = \frac{\rho_0}{d_{k\mathrm{B}}^2[n]} = \frac{\rho_0}{\|\mathbf{w}_k - \mathbf{q}_{\mathrm{B}}[n]\|^2 + H^2}, \tag{1}$$

where ρ_0 denotes the channel power gain at the reference distance 1 m, $d_{k\mathrm{B}}[n]$ is the distance between the kth Alice and Bob in time slot $n \in \{1, \ldots, N\}$, and $\mathbf{w}_k \in \mathbb{R}^{2\times 1}$ represents the horizontal location of the kth Alice. Similarly, the jamming channel power gains from Jack to Bob and Eve can be written as $g_{\mathrm{JB}}[n] = \frac{\rho_0}{\|\mathbf{q}_{\mathrm{J}}[n]-\mathbf{q}_{\mathrm{B}}[n]\|^2}$ and $g_{\mathrm{JE}}[n] = \frac{\rho_0}{\|\mathbf{q}_{\mathrm{J}}[n]-\mathbf{w}_{\mathrm{E}}\|^2+H^2}$, respectively. $\mathbf{w}_{\mathrm{E}} \in \mathbb{R}^{2\times 1}$ denotes the horizontal location of Eve. However, Eve needs to hide itself from detection and its accurate location is unknown to the legitimate network. Nevertheless, all the devices can approximately estimate it within a circle, i.e., with $\tilde{\mathbf{w}}_{\mathrm{E}} \in \mathbb{R}^{2\times 1}$ and r_{E} as the center and radius, respectively. Accordingly, we have $\|\tilde{\mathbf{w}}_{\mathrm{E}} - \mathbf{w}_{\mathrm{E}}\| \le r_{\mathrm{E}}$. In practice, we assume that the uncertainty region r_{E} is usually smaller than the distance between Eve and Alice, i.e., $\|\mathbf{w}_k - \tilde{\mathbf{w}}_{\mathrm{E}}\| \ge r_{\mathrm{E}}$.

For the ground wiretap channel from the kth Alice to Eve, we consider both large-scale path-loss and small-scale Rayleigh fading. The channel power gain can be expressed as

$$g_{k\mathrm{E}} = \frac{\rho_0}{d_{k\mathrm{E}}^{\alpha}}\zeta = \frac{\rho_0}{\|\mathbf{w}_k - \mathbf{w}_{\mathrm{E}}\|^{\alpha}}\zeta, \tag{2}$$

where ζ follows an exponential distribution with unit mean and $\alpha > 2$ denotes the path-loss exponent.

Denote the scheduling variable $s_k[n] = 1$ when the kth ground node is enabled to communicate with Bob at the nth time slot, while other nodes keep silence. Otherwise, $s_k[n] = 0$. Assume that at most one ground node can send its data to Bob in each time slot. Thus, we have

$$\sum\nolimits_{k=1}^{K} s_k[n] \le 1, \forall n, \quad s_k[n] \in \{0,1\}, \forall k, n. \tag{3}$$

Let $p_k[n]$ and $p_{\mathrm{J}}[n]$ denote the transmit power of the kth Alice and Jack in the nth time slot, respectively. Thus, the achievable rate per Hz from the kth Alice to Bob in time slot n can be expressed as

$$R_{k\mathrm{B}}[n] = s_k[n]\log_2\left(1 + \frac{p_k[n]g_{k\mathrm{B}}[n]}{p_{\mathrm{J}}[n]g_{\mathrm{JB}}[n] + \sigma_{\mathrm{B}}^2}\right), \tag{4}$$

where σ_{B}^2 is the additive white Gaussian noise (AWGN) power at Bob. Similarly, the achievable rate per Hz at Eve in time slot n can be obtained as

$$R_{k\mathrm{E}}[n] = s_k[n]\mathbb{E}_{\zeta}\left[\log_2\left(1 + \frac{p_k[n]g_{k\mathrm{E}}}{p_{\mathrm{J}}[n]g_{\mathrm{JE}}[n] + \sigma_{\mathrm{E}}^2}\right)\right], \tag{5}$$

where $\mathbb{E}_{\zeta}[\cdot]$ denotes the expectation with respect to the random variable ζ.

In order to evaluate the secrecy performance of the kth Alice, we adopt the average secrecy rate (ASR) per Hz over the N time slots as

$$\bar{R}_{\mathrm{sec}}^{k} = \frac{1}{N}\sum_{n=1}^{N} R_{\mathrm{sec}}^{k}[n] = \frac{1}{N}\sum_{n=1}^{N}\Big[R_{k\mathrm{B}}[n] - R_{k\mathrm{E}}[n]\Big]^{+}, \tag{6}$$

where $[x]^{+} \triangleq \max(x, 0)$. The total information bits transmitted from the kth Alice is defined as $B_w\delta_t\sum_{n=1}^{N} R_{\mathrm{sec}}^{k}[n]$, and B_w represents the bandwidth. Furthermore, the energy consumption is one of the crucial and indispensable modules to affect the UAV endurance, which should be considered. For a rotary-wing UAV with speed $\mathbf{v}_i[n]$, the propulsion power consumption can be approximated as [14]

$$\begin{aligned} P_{\mathrm{prop}}^{i}[n] = &\underbrace{P_0\left(1 + \frac{3\|\mathbf{v}_i[n]\|^2}{\Omega^2 r^2}\right)}_{\text{blade profile}} + \underbrace{\frac{1}{2}d_0\rho s A\|\mathbf{v}_i[n]\|^3}_{\text{parasite}} \\ &+ \underbrace{P_i\left(\sqrt{1 + \frac{\|\mathbf{v}_i[n]\|^4}{4v_0^4}} - \frac{\|\mathbf{v}_i[n]\|^2}{2v_0^2}\right)^{\frac{1}{2}}}_{\text{induced}}, \forall i \in \{\mathrm{B}, \mathrm{J}\}, \forall n, \end{aligned} \tag{7}$$

where P_0 and P_i are two constants denoting the intrinsic blade profile power and the induced power when $\mathbf{v}_i[n] = 0$, respectively, Ω and r are the blade angular velocity and the rotor radius, respectively, d_0 and ρ denote the fuselage drag

[1]According to an extensive survey for UAV channel modeling [40], [41], if the UAV is located high enough, e.g., above 120 m, the LoS probability can be approximate to 1.

ratio and the air density, respectively, s and A denote the rotor solidity and the rotor disc area, respectively, and the mean rotor induced velocity is represented as v_0. Thus, we can calculate the average propulsion power and the total consumed propulsion energy over N time slots as $\frac{1}{N}\sum_{i\in\{\mathrm{B,J}\}}\sum_{n=1}^{N}P^i_{\mathrm{prop}}[n]$ and $\delta_t\sum_{i\in\{\mathrm{B,J}\}}\sum_{n=1}^{N}P^i_{\mathrm{prop}}[n]$, respectively. The power consumption of system contains two parts, i.e., the propulsion power and the signal processing power. The transmit power and the power consumed by the electric circuits and channel decoders of the legitimate nodes can be ignored because they are much lower than the propulsion power (usually less than 1%). Thus, we define the ratio between the information bits transmitted among the nodes and the total energy consumed of the UAVs as the secrecy energy efficiency (SEE), which can be given by

$$\mathrm{EE}_{\mathrm{sec}}(\mathbf{S},\mathbf{P},\mathbf{B},\mathbf{J})=\frac{B_w\sum_{k=1}^{K}\sum_{n=1}^{N}R^k_{\mathrm{sec}}[n]}{\sum_{i\in\{\mathrm{B,J}\}}\sum_{n=1}^{N}P^i_{\mathrm{prop}}[n]}, \tag{8}$$

where $\mathbf{S}\triangleq\{s_k[n],\forall k,n\}$, $\mathbf{P}\triangleq\{p_k[n],p_{\mathrm{J}}[n],\forall k,n\}$, $\mathbf{B}\triangleq\{\mathbf{q}_{\mathrm{B}}[n],\mathbf{v}_{\mathrm{B}}[n],\forall n\}$, $\mathbf{J}\triangleq\{\mathbf{q}_{\mathrm{J}}[n],\mathbf{v}_{\mathrm{J}}[n],\forall n\}$.

In this paper, we first maximize the sum ASR among the nodes with the average propulsion limitation in Section III. This happens when the battery capacity is known to us and we want to collect as much data as possible in a small flight mission. If we need to prolong the UAV endurance and support all of the individual nodes, the SEE should be considered. Then, we further maximize the SEE in Section IV.

III. Optimization for Maximizing Sum ASR

In this section, we aim to maximize the sum ASR via jointly optimizing the scheduling and the trajectory of UAVs as well as the transmit power with propulsion limitation. The BCD method is applied to optimize the scheduling $\mathbf{S}$, the transmit power allocation $\mathbf{P}$, the trajectory and velocity of the two UAVs Bob $\mathbf{B}$ and Jack $\mathbf{J}$, alternately.

A. Problem Formulation

This optimization problem can be formulated as

$$\begin{aligned}
(\mathrm{P1}):\ &\max_{\mathbf{S},\mathbf{P},\mathbf{B},\mathbf{J}}\ \sum_{k=1}^{K}\bar{R}^k_{\mathrm{sec}} \qquad (9)\\
&s.t.\ \ \mathrm{C1}:\sum_{k=1}^{K}s_k[n]\le 1,\forall n,\\
&\quad\mathrm{C2}: s_k[n]\in\{0,1\},\forall k,n,\\
&\quad\mathrm{C3}:\bar{R}^k_{\mathrm{sec}}\ge R_{\min},\forall k,\\
&\quad\mathrm{C4}:\frac{1}{N}\sum_{n=1}^{N}\sum_{k=1}^{K}s_k[n]p_k[n]\le P^{\mathrm{A}}_{\mathrm{ave}},\\
&\quad\mathrm{C5}: 0\le p_k[n]\le P^{\mathrm{A}}_{\max},\forall k,n,\\
&\quad\mathrm{C6}:\frac{1}{N}\sum_{n=1}^{N}p_{\mathrm{J}}[n]\le P^{\mathrm{J}}_{\mathrm{ave}},\\
&\quad\mathrm{C7}: 0\le p_{\mathrm{J}}[n]\le P^{\mathrm{J}}_{\max},\forall n,\\
&\quad\mathrm{C8}:\frac{1}{N}\sum_{i\in\{\mathrm{B,J}\}}\sum_{n=1}^{N}P^i_{\mathrm{prop}}[n]\le P_{\mathrm{lim}},\\
&\quad\mathrm{C9}:\mathbf{q}_i[n+1]=\mathbf{q}_i[n]+\mathbf{v}_i[n]\delta_t,\\
&\qquad\qquad n=1,...,N-1,\forall i\in\{\mathrm{B,J}\},\\
&\quad\mathrm{C10}:\mathbf{q}_i[0]=\mathbf{q}_{i,I},\mathbf{q}_i[N]=\mathbf{q}_{i,F},\forall i\in\{\mathrm{B,J}\},\\
&\quad\mathrm{C11}:\|\mathbf{q}_{\mathrm{B}}[n]-\mathbf{q}_{\mathrm{J}}[n]\|\ge\widetilde{D},\forall n,\\
&\quad\mathrm{C12}:\|\mathbf{v}_i[n]\|\le V_{\max},\forall n,\forall i\in\{\mathrm{B,J}\},\\
&\quad\mathrm{C13}:\|\mathbf{v}_i[n+1]-\mathbf{v}_i[n]\|\le a_{\max},\forall n,\forall i\in\{\mathrm{B,J}\},
\end{aligned}$$

where C1 and C2 are the scheduling constraints of ground nodes. $R_{\min}$ in C3 is the minimum required ASR of each ground user over the whole flight, which can guarantee the fairness among users when properly set. (C4, C6) and (C5, C7) are the constraints of average and peak transmit/jamming powers in each time slot. We take the average propulsion power budget of UAV as P_{lim} in C8, according to the battery capacity. C9 approximately holds, when the trajectory in each time slot can be deemed as a straight line due to the small δ_t. The initial and final locations of UAVs are assumed in C10. For the dual-UAV system, collision avoidance should be considered in C11. In addition, C12 and C13 are velocity restrictions. Each UAV can adjust its velocity from one slot to the next, and $V_{\max}$ stands for the maximum UAV speed and $a_{\max}$ is the maximum acceleration.

Notice that (P1) is non-convex due to the objective function, the non-convex constraints C3, C8 and C11, and non-smooth operator $[\cdot]^+$. The non-smoothness of the objective function should be handled first. If the term $R_{k\mathrm{B}}[n]-R_{k\mathrm{E}}[n]$ in (6) is a negative value at time slot n, we can set $p_k[n]=0$, which results in $R^k_{\mathrm{sec}}[n]=0$. Therefore, the secrecy rate is always non-negative via optimizing the transmit power. The operator $[\cdot]^+$ can be removed and without changing the optimal solution to the original problem.

$R_{k\mathrm{E}}[n]$ in the objective function is implicit due to the expectation with respect to the random variable ζ and the location uncertainty of Eve. To simplify the derivation, we maximize the sum ASR in the worst case. In Lemma 1, we approximate $R_{k\mathrm{E}}[n]$ and obtain an upper bound of the achievable rate from the kth Alice to Eve.

Lemma 1: The upper bound of $R_{k\mathrm{E}}[n]$ can be given by

$$R_{k\mathrm{E}}[n] \leq \hat{R}_{k\mathrm{E}}[n] = s_k[n]\log_2\left(1+\frac{p_k[n]\hat{g}_{k\mathrm{E}}}{p_{\mathrm{J}}[n]\hat{g}_{\mathrm{JE}}[n]+\sigma_{\mathrm{E}}^2}\right), \quad (10)$$

where $\hat{g}_{k\mathrm{E}}$ and $\hat{g}_{\mathrm{JE}}[n]$ can be denoted as

$$\hat{g}_{k\mathrm{E}} = \rho_0\left(\|\mathbf{w}_k - \tilde{\mathbf{w}}_{\mathrm{E}}\| - r_{\mathrm{E}}\right)^{-\alpha}, \forall n, \quad (11)$$

$$\hat{g}_{\mathrm{JE}}[n] = \rho_0\left(\left(\|\mathbf{q}_{\mathrm{J}}[n] - \tilde{\mathbf{w}}_{\mathrm{E}}\| + r_{\mathrm{E}}\right)^2 + H^2\right)^{-1}. \quad (12)$$

Proof: Please refer to Appendix A. ∎

Based on Lemma 1, we obtain the ASR of the kth Alice in the worst case, which can be defined as

$$\eta^k = \frac{1}{N}\sum_{n=1}^{N}(R_{k\mathrm{B}}[n] - \hat{R}_{k\mathrm{E}}[n]), \quad (13)$$

where η^k is a function of $\mathbf{S}$, $\mathbf{P}$, $\mathbf{B}$ and $\mathbf{J}$. The sum ASR $\sum_{k=1}^{K}\eta^k$ will be maximized in the following subsections.

B. Subproblems 1 & 2: Scheduling and Transmit Power Optimization

In this subsection, we first optimize the scheduling variable $\mathbf{S}$ for fixed feasible power and trajectory. This is an integer optimization problem. To handle the binary constraint C2, the binary variable $s_k[n]$ is relaxed into a real value $\tilde{s}_k[n]$ between 0 and 1. Thus, (P1) can be reduced to a standard linear programming problem because the objective function and the constraints are linear with respect to $\mathbf{S}$. We formulate the first subproblem as

$$\begin{aligned}
(\mathrm{P2}): \max_{\mathbf{S},\eta^k} \quad & \sum\nolimits_{k=1}^{K}\eta^k && (14a)\\
s.t. \quad & \frac{1}{N}\sum_{n=1}^{N}(R_{k\mathrm{B}}[n] - \hat{R}_{k\mathrm{E}}[n]) \geq \eta^k, \forall k, && (14b)\\
& \eta^k \geq R_{\min}, \forall k, && (14c)\\
& \sum\nolimits_{k=1}^{K}\tilde{s}_k[n] \leq 1, \forall n, && (14d)\\
& 0 \leq \tilde{s}_k[n] \leq 1, \forall n, k. && (14e)
\end{aligned}$$

(P2) can be solved by classical convex optimization tools, e.g., CVX. Then, the solution $\mathbf{S}$ obtained from (P2) needs to be reconstructed as a binary variable according to [12].

Then, we aim at optimizing the information transmit power of the kth Alice and the jamming power of Jack with all the other variables unchanged. The subproblem can be expressed as

$$\begin{aligned}
(\mathrm{P3}): \max_{\mathbf{P},\eta^k} \quad & \sum\nolimits_{k=1}^{K}\eta^k && (15a)\\
s.t. \quad & \frac{1}{N}\sum_{n=1}^{N}s_k[n]\hat{R}_k[n] \geq \eta^k, \forall k, && (15b)\\
& \eta^k \geq R_{\min}, \forall k, && (15c)\\
& \mathrm{C4}-\mathrm{C7}, && (15d)
\end{aligned}$$

where

$$\begin{aligned}
\hat{R}_k[n] = {} & \log_2(p_k[n]g_{k\mathrm{B}}[n] + p_{\mathrm{J}}[n]g_{\mathrm{JB}}[n] + \sigma_{\mathrm{B}}^2)\\
& - \log_2(p_{\mathrm{J}}[n]g_{\mathrm{JB}}[n] + \sigma_{\mathrm{B}}^2) + \log_2(p_{\mathrm{J}}[n]\hat{g}_{\mathrm{JE}}[n] + \sigma_{\mathrm{E}}^2) \quad (16)\\
& - \log_2(p_{\mathrm{J}}[n]\hat{g}_{\mathrm{JE}}[n] + p_k[n]\hat{g}_{k\mathrm{E}} + \sigma_{\mathrm{E}}^2).
\end{aligned}$$

(15b) is a non-convex constraint due to the fact that the second and fourth terms in $\hat{R}_k[n]$ are convex functions with respect to p_k and p_{J}. To tackle the non-convex problem, we apply the first-order restrictive approximation to transform $\hat{R}_k[n]$ into a concave function. The transformation is presented in the following inequality, where $\{\widetilde{p}_k[n], \widetilde{p}_{\mathrm{J}}[n], \forall k, n\}$ is a given feasible point.

$$\begin{aligned}
& \log_2(p_{\mathrm{J}}[n]\hat{g}_{\mathrm{JE}}[n] + p_k[n]\hat{g}_{k\mathrm{E}} + \sigma_{\mathrm{E}}^2) + \log_2(p_{\mathrm{J}}[n]g_{\mathrm{JB}}[n] + \sigma_{\mathrm{B}}^2)\\
& \leq f_1(p_k[n], p_{\mathrm{J}}[n], \widetilde{p}_k[n], \widetilde{p}_{\mathrm{J}}[n]).
\end{aligned} \quad (17)$$

with $f_1(p_k[n], p_{\mathrm{J}}[n], \widetilde{p}_k[n], \widetilde{p}_{\mathrm{J}}[n])$ in (17) shown in (18) at the top of the next page.

For given feasible local point $\{\widetilde{p}_k[n], \widetilde{p}_{\mathrm{J}}[n]\}$, $f_1(p_k[n], p_{\mathrm{J}}[n], \widetilde{p}_k[n], \widetilde{p}_{\mathrm{J}}[n])$ is a convex function with respect to the optimization variables $p_k[n]$ and $p_{\mathrm{J}}[n]$. Thus, the original problem (P3) can be approximated as

$$\begin{aligned}
(\mathrm{P3.1}): \max_{\mathbf{P},\eta_p^k} \quad & \sum_{k=1}^{K}\eta_p^k && (19a)\\
s.t. \quad & \frac{1}{N}\sum_{n=1}^{N}s_k[n]\Big(\hat{R}_1[n] - f_1(p_k[n], p_{\mathrm{J}}[n], \widetilde{p}_k[n], \widetilde{p}_{\mathrm{J}}[n])\Big)\\
& \geq \eta_p^k, \forall k, && (19b)\\
& \eta_p^k \geq R_{\min}, \forall k, && (19c)\\
& \mathrm{C4}-\mathrm{C7}, && (19d)
\end{aligned}$$

where $\sum_{k=1}^{K}\eta_p^k$ is the objective function of (P3.1) and $\hat{R}_1[n]$ is the sum of the first and third terms in $\hat{R}_k[n]$. Therefore, the problem (P3.1) is convex and can be solved by CVX. After initialization, $\{\widetilde{p}_k[n], \widetilde{p}_{\mathrm{J}}[n], \forall k, n\}$ is updated with the optimized $\mathbf{P}$ of (P3.1) in each iteration.

C. Subproblem 3: Optimizing Bob's Trajectory and Velocity

Then, we optimize Bob's trajectory $\mathbf{q}_{\mathrm{B}}[n]$ and velocity $\mathbf{v}_{\mathrm{B}}[n]$ with given user scheduling $\mathbf{S}$, the transmit power allocation $\mathbf{P}$, and the trajectory and velocity of Jack. The subproblem can be expressed as

$$\begin{aligned}
(\mathrm{P4}): \max_{\mathbf{B},\eta^k} \quad & \sum_{k=1}^{K}\eta^k && (20a)\\
s.t. \quad & \frac{1}{N}\sum_{n=1}^{N}\left(s_k[n]\log_2\left(1+\frac{p_k[n]g_{k\mathrm{B}}[n]}{p_{\mathrm{J}}[n]g_{\mathrm{JB}}[n]+\sigma_{\mathrm{B}}^2}\right) - \hat{R}_{k\mathrm{E}}[n]\right)\\
& \geq \eta^k, \forall k, && (20b)\\
& \eta^k \geq R_{\min}, \forall k, && (20c)\\
& \mathrm{C8}-\mathrm{C13}. && (20d)
\end{aligned}$$

Since the left-hand-side of (20b) is non-concave and C8 and C11 are non-convex, the optimization problem is non-convex and difficult to solve. To facilitate the derivation, we introduce auxiliary variables $\{H_k[n] = \frac{(\|\mathbf{w}_k - \mathbf{q}_{\mathrm{B}}[n]\|^2 + H^2)\sigma_{\mathrm{B}}^2}{p_k[n]\rho_0}, \forall k, n\}$, $\{I[n] = \frac{p_{\mathrm{J}}[n]\rho_0}{\sigma_{\mathrm{B}}^2}D[n]^{-1} + 1, \forall n\}$ and $\{D[n] = \|\mathbf{q}_{\mathrm{J}}[n] - \mathbf{q}_{\mathrm{B}}[n]\|^2, \forall n\}$. Thus, the problem (P4)

$$f_1(p_k[n],p_{\rm J}[n],\widetilde{p}_k[n],\widetilde{p}_{\rm J}[n]) \triangleq \frac{\hat{g}_{\rm JE}[n](p_{\rm J}[n]-\widetilde{p}_{\rm J}[n])+\hat{g}_{ke}(p_k[n]-\widetilde{p}_k[n])}{\ln 2(\widetilde{p}_{\rm J}[n]\hat{g}_{\rm JE}[n]+\widetilde{p}_k[n]\hat{g}_{\rm kE}+\sigma_{\rm E}^2)}+\log_2(\widetilde{p}_{\rm J}[n]\hat{g}_{\rm JE}[n]+\widetilde{p}_k[n]\hat{g}_{\rm kE}+\sigma_{\rm E}^2) + \frac{g_{\rm JB}[n](p_{\rm J}[n]-\widetilde{p}_{\rm J}[n])}{\ln 2(\widetilde{p}_{\rm J}[n]g_{\rm JB}[n]+\sigma_{\rm B}^2)}+\log_2(\widetilde{p}_{\rm J}[n]g_{\rm JB}[n]+\sigma_{\rm B}^2),\forall k,n. \tag{18}$$

can be changed into

$$(\text{P4.1}): \max_{\substack{\mathbf{B},\eta^k,H_k[n],\\ I[n],D[n]}} \sum_{k=1}^{K}\eta^k \tag{21a}$$

$$s.t.\ \frac{1}{N}\sum_{n=1}^{N}\left(s_k[n]\log_2\left(1+\frac{1}{H_k[n]I[n]}\right)-\hat{R}_{\rm kE}[n]\right)\geq\eta^k, \tag{21b}$$

$$\eta^k \geq R_{\min},\forall k, \tag{21c}$$

$$\frac{1}{N}\sum_{n=1}^{N}\left(P_{\rm prop}^{\rm B}[n]+P_{\rm prop}^{\rm J}[n]\right)\leq P_{\lim}, \tag{21d}$$

$$\|\mathbf{q}_{\rm B}[n]-\mathbf{q}_{\rm J}[n]\|\geq\widetilde{D},\forall n, \tag{21e}$$

$$H_k[n]\geq\frac{(\|\mathbf{w}_k-\mathbf{q}_{\rm B}[n]\|^2+H^2)\sigma_{\rm B}^2}{p_k[n]\rho_0},\forall k,n, \tag{21f}$$

$$I[n]\geq p_{\rm J}[n]\rho_0 D[n]^{-1}/\sigma_{\rm B}^2+1,\forall n, \tag{21g}$$

$$D[n]\leq\|\mathbf{q}_{\rm J}[n]-\mathbf{q}_{\rm B}[n]\|^2,\forall n, \tag{21h}$$

$$\text{C9}-\text{C10},\text{C12}-\text{C13}. \tag{21i}$$

Note that (21f) should achieve equality at the optimal point, otherwise decreasing $H_k[n]$ can increase the value of the objective function. This is also the case for (21g) and (21h). Thus, the problems (P4.1) and (P4) have the same optimal solution. However, the problem (P4.1) is still non-convex owing to the non-convex constraints (21b), (21d), (21e) and (21h). Based on the types of optimization variables, we divide these non-convex constraints into two parts to transform.

1) Constraints (21b), (21e) and (21h): To address the non-convex constraint (21b), we introduce the following lemma.

Lemma 2: The lower bound of $\log_2\left(1+\frac{1}{H_k[n]I[n]}\right)$ at the given local point $\{\widetilde{H}_k[n],\widetilde{I}[n]\}$ can be expressed as

$$\log_2\left(1+\frac{1}{H_k[n]I[n]}\right)\geq f_2(H_k[n],I[n],\widetilde{H}_k[n],\widetilde{I}[n]), \tag{22}$$

where

$$f_2(H_k[n],I[n],\widetilde{H}_k[n],\widetilde{I}[n])\triangleq\log_2\left(1+\frac{1}{\widetilde{H}_k[n]\widetilde{I}[n]}\right) -\frac{H_k[n]-\widetilde{H}_k[n]}{\ln 2(\widetilde{H}_k[n]+\widetilde{H}_k[n]^2\widetilde{I}[n])}-\frac{I[n]-\widetilde{I}[n]}{\ln 2(\widetilde{I}[n]+\widetilde{I}[n]^2\widetilde{H}_k[n])}. \tag{23}$$

Proof: Please refer to Appendix B. ∎

Based on Lemma 2, the constraint (21b) can be transformed into a non-convex one, which can be rewritten as

$$\frac{1}{N}\sum_{n=1}^{N}\left(s_k[n]f_2(H_k[n],I[n],\widetilde{H}_k[n],\widetilde{I}[n])-\hat{R}_{\rm kE}[n]\right)\geq\eta^k. \tag{24}$$

Furthermore, we apply SCA to obtain the lower bound of the norm-squared function in (21e) and (21h) as

$$\|\mathbf{q}_{\rm B}[n]-\mathbf{q}_{\rm J}[n]\|^2\geq\|\widetilde{\mathbf{q}}_{\rm B}[n]-\mathbf{q}_{\rm J}[n]\|^2 +2(\widetilde{\mathbf{q}}_{\rm B}[n]-\mathbf{q}_{\rm J}[n])^T(\mathbf{q}_{\rm B}[n]-\widetilde{\mathbf{q}}_{\rm B}[n])\triangleq f_3(\mathbf{q}_{\rm B}[n],\widetilde{\mathbf{q}}_{\rm B}[n]), \tag{25}$$

where $\widetilde{\mathbf{q}}_{\rm B}[n]$ is the given local point, and $f_3(\mathbf{q}_{\rm B}[n],\widetilde{\mathbf{q}}_{\rm B}[n])$ in (25) is a linear function with respect to the variable $\mathbf{q}_{\rm B}[n]$. Thus, (21e) and (21h) are approximately convex.

2) Propulsion Power Constraint (21d): The constraint (21d) is non-convex and the third term in $P_{\rm prop}^{\rm B}[n]$ is mathematically intractable. We introduce a slack variable $\{\lambda_{\rm B}[n]\geq 0\}$ as

$$\lambda_{\rm B}[n]=\left(\sqrt{1+\frac{\|\mathbf{v}_{\rm B}[n]\|^4}{4v_0^4}}-\frac{\|\mathbf{v}_{\rm B}[n]\|^2}{2v_0^2}\right)^{1/2},\forall n, \tag{26}$$

and (26) can be relaxed into an inequality constraint as

$$\frac{1}{\lambda_{\rm B}[n]^2}\leq\lambda_{\rm B}[n]^2+\frac{\|\mathbf{v}_{\rm B}[n]\|^2}{v_0^2},\forall n. \tag{27}$$

Note that the constraint (27) should be met with equality. This is because we can always decrease $\lambda_{\rm B}[n]$ with other variables fixed, yet without changing the objective value of (P4). The right-hand-side of (27) is jointly convex with respect to $\lambda_{\rm B}[n]$ and $\mathbf{v}_{\rm B}[n]$, and we can adopt the first-order Taylor expansion at the given feasible point $\{\widetilde{\lambda}_{\rm B}[n],\widetilde{\mathbf{v}}_{\rm B}[n]\}$ as

$$\lambda_{\rm B}[n]^2+\frac{\|\mathbf{v}_{\rm B}[n]\|^2}{v_0^2}\geq f_4(\lambda_{\rm B}[n],\mathbf{v}_{\rm B}[n],\widetilde{\lambda}_{\rm B}[n],\widetilde{\mathbf{v}}_{\rm B}[n]), \tag{28}$$

where

$$f_4(\lambda_{\rm B}[n],\mathbf{v}_{\rm B}[n],\widetilde{\lambda}_{\rm B}[n],\widetilde{\mathbf{v}}_{\rm B}[n])\triangleq 2\widetilde{\lambda}_{\rm B}[n](\lambda_{\rm B}[n]-\widetilde{\lambda}_{\rm B}[n]) +\widetilde{\lambda}_{\rm B}[n]^2+\frac{\|\widetilde{\mathbf{v}}_{\rm B}[n]\|^2}{v_0^2}+\frac{2}{v_0^2}(\widetilde{\mathbf{v}}_{\rm B}[n])^T(\mathbf{v}_{\rm B}[n]-\widetilde{\mathbf{v}}_{\rm B}[n]). \tag{29}$$

As such, the constraint (27) can be rewritten as

$$\frac{1}{\lambda_{\rm B}[n]^2}\leq f_4(\lambda_{\rm B}[n],\mathbf{v}_{\rm B}[n],\widetilde{\lambda}_{\rm B}[n],\widetilde{\mathbf{v}}_{\rm B}[n]),\forall n, \tag{30}$$

which is convex.

Finally, we have transformed these non-convex constraints into convex ones, and the problem (P4.1) can be approximated

as

$$(\text{P4.2}): \max_{\substack{\mathbf{B},\eta_{\text{B}}^k,H_k[n],\\ I[n],D[n],\lambda_{\text{B}}[n]}} \sum_{k=1}^{K} \eta_{\text{B}}^k \tag{31a}$$

$$s.t.\ \frac{1}{N}\sum_{n=1}^{N}\Big(s_k[n]f_2(H_k[n],I[n],\widetilde{H}_k[n],\widetilde{I}[n])-\hat{R}_{k\text{E}}[n]\Big)\geq\eta_{\text{B}}^k \tag{31b}$$

$$f_3(\mathbf{q}_{\text{B}}[n],\widetilde{\mathbf{q}}_{\text{B}}[n]) \geq \widetilde{D}^2, \forall n, \tag{31c}$$

$$D[n] \leq f_3(\mathbf{q}_{\text{B}}[n],\widetilde{\mathbf{q}}_{\text{B}}[n]), \forall n, \tag{31d}$$

$$\frac{1}{\lambda_{\text{B}}[n]^2} \leq f_4(\lambda_{\text{B}}[n],\mathbf{v}_{\text{B}}[n],\widetilde{\lambda}_{\text{B}}[n],\widetilde{\mathbf{v}}_{\text{B}}[n]), \forall n, \tag{31e}$$

$$\frac{1}{N}\sum_{n=1}^{N}\left(f_5(\lambda_{\text{B}}[n],\mathbf{v}_{\text{B}}[n])+P_{\text{prop}}^{\text{J}}[n]\right) \leq P_{\lim}, \tag{31f}$$

$$(21\text{c}),(21\text{f}),(21\text{g}),(21\text{i}), \tag{31g}$$

where $\sum_{k=1}^{K}\eta_{\text{B}}^k$ is the objective function of (P4.2) and $f_5(\lambda_{\text{B}}[n],\mathbf{v}_{\text{B}}[n])$ can be expressed as

$$f_5(\lambda_{\text{B}}[n],\mathbf{v}_{\text{B}}[n]) \triangleq P_0\left(1+\frac{3\|\mathbf{v}_{\text{B}}[n]\|^2}{\Omega^2 r^2}\right)+\frac{1}{2}d_0\rho s A\|\mathbf{v}_{\text{B}}[n]\|^3 + P_i\lambda_{\text{B}}[n]. \tag{32}$$

Thus, the problem (P4.2) is a standard convex optimization. With given feasible points, it can be solved by CVX.

D. Subproblem 4: Optimizing Jack's Trajectory and Velocity

Finally, we optimize Jack's trajectory $\mathbf{q}_{\text{J}}[n]$ and velocity $\mathbf{v}_{\text{J}}[n]$ with other variables fixed. Similarly, the optimization problem is intractable due to the non-convexity. Thus, we introduce the slack variables $\{X[n]=\frac{\rho_0}{\sigma_{\text{B}}^2(\|\mathbf{q}_{\text{J}}[n]-\mathbf{q}_{\text{B}}[n]\|^2)},\forall n\}$ and $\{Y[n]=\frac{\rho_0}{\sigma_{\text{E}}^2\left((\|\mathbf{q}_{\text{J}}[n]-\tilde{\mathbf{w}}_{\text{E}}\|+r_{\text{E}})^2+H^2\right)},\forall n\}$. Accordingly, we can obtain the optimization problem as

$$(\text{P5}): \max_{\mathbf{J},\eta^k} \sum_{k=1}^{K}\eta^k \tag{33a}$$

$$s.t.\ \frac{1}{N}\sum_{n=1}^{N}s_k[n]\log_2\left(\frac{1+\frac{a_k[n]}{p_{\text{J}}[n]X[n]+1}}{1+\frac{b_k[n]}{p_{\text{J}}[n]Y[n]+1}}\right)\geq\eta^k, \tag{33b}$$

$$\frac{1}{N}\sum_{n=1}^{N}\left(P_{\text{prop}}^{\text{J}}[n]+P_{\text{prop}}^{\text{B}}[n]\right)\leq P_{\lim}, \tag{33c}$$

$$\|\mathbf{q}_{\text{J}}[n]-\mathbf{q}_{\text{B}}[n]\|\geq\widetilde{D},\forall n, \tag{33d}$$

$$\frac{1}{X[n]}\leq\frac{\sigma_{\text{B}}^2\|\mathbf{q}_{\text{J}}[n]-\mathbf{q}_{\text{B}}[n]\|^2}{\rho_0},\forall n, \tag{33e}$$

$$\frac{1}{Y[n]}\geq\frac{\sigma_{\text{E}}^2\left(\left(\|\mathbf{q}_{\text{J}}[n]-\tilde{\mathbf{w}}_{\text{E}}\|+r_{\text{E}}\right)^2+H^2\right)}{\rho_0},\forall n, \tag{33f}$$

$$\eta^k\geq R_{\min},\forall k, \tag{33g}$$

$$\text{C9}-\text{C10},\text{C12}-\text{C13}, \tag{33h}$$

where $a_k[n]=\frac{p_k[n]g_{k\text{B}}[n]}{\sigma_{\text{B}}^2}$ and $b_k[n]=\frac{p_k[n]\hat{g}_{k\text{E}}}{\sigma_{\text{E}}^2}$.

Problem (P5) is still non-convex due to the constraints (33b)-(33f). Without loss of generality, the constraints (33e) and (33f) achieve equality at the optimal point. The reason is similar to other slack variables such as $\{H_k[n]\}$ and $\{I[n]\}$. Notice that the non-convex constraints (33c)-(33f) can be solved in similar methods to the previous subsection. In the following, we will focus on tackling the constraint (33b), with the following lemma first presented.

Lemma 3: If $a_k[n]$ is a nonnegative parameter, the following inequality must hold.

$$\log_2\left(1+\frac{a_k[n]}{p_{\text{J}}[n]X[n]+1}\right)\geq f_6(X[n],\widetilde{X}[n]), \tag{34}$$

where $f_6(X[n],\widetilde{X}[n])$ is shown at the top of the next page, and $\{\widetilde{X}[n]\}$ is the given feasible point.

Proof: Please refer to Appendix C. ■

According to Lemma 3, the constraint (33b) can be rewritten as

$$\frac{1}{N}\sum_{n=1}^{N}s_k[n]\left(f_6(X[n],\widetilde{X}[n])-\log_2\left(1+\frac{b_k[n]}{p_{\text{J}}[n]Y[n]+1}\right)\right)\geq\eta^k. \tag{36}$$

According to the above discussions, the original problem (P5) can be approximated as

$$(\text{P5.1}): \max_{\substack{\mathbf{J},\eta_{\text{J}}^k,X[n],\\ Y[n],\lambda_{\text{J}}[n]}} \sum_{k=1}^{K}\eta_{\text{J}}^k \tag{37a}$$

$$s.t.\ \frac{1}{N}\sum_{n=1}^{N}s_k[n]\left(f_6(X[n],\widetilde{X}[n])-\log_2\left(1+\frac{b_k[n]}{p_{\text{J}}[n]Y[n]+1}\right)\right) \geq\eta_{\text{J}}^k, \tag{37b}$$

$$f_3(\mathbf{q}_{\text{J}}[n],\widetilde{\mathbf{q}}_{\text{J}}[n])\geq\widetilde{D}^2,\forall n, \tag{37c}$$

$$\frac{\rho_0}{\sigma_{\text{B}}^2X[n]}\leq f_3(\mathbf{q}_{\text{J}}[n],\widetilde{\mathbf{q}}_{\text{J}}[n]),\forall n, \tag{37d}$$

$$\frac{1}{\lambda_{\text{J}}[n]^2}\leq f_4(\lambda_{\text{J}}[n],\mathbf{v}_{\text{J}}[n],\widetilde{\lambda}_{\text{J}}[n],\widetilde{\mathbf{v}}_{\text{J}}[n]),\forall n, \tag{37e}$$

$$\frac{1}{N}\sum_{n=1}^{N}\left(f_5(\lambda_{\text{J}}[n],\mathbf{v}_{\text{J}}[n])+P_{\text{prop}}^{\text{B}}[n]\right)\leq P_{\lim}, \tag{37f}$$

$$\frac{\rho_0 f_7(Y[n],\widetilde{Y}[n])}{\sigma_{\text{E}}^2}\geq(\|\mathbf{q}_{\text{J}}[n]-\tilde{\mathbf{w}}_{\text{E}}\|+r_{\text{E}})^2+H^2,\forall n, \tag{37g}$$

$$(33\text{g}),(33\text{h}), \tag{37h}$$

where $\sum_{k=1}^{K}\eta_{\text{J}}^k$ is the objective value of (P5.1), and $f_7(Y[n],\widetilde{Y}[n])$ can be expressed as

$$f_7(Y[n],\widetilde{Y}[n])\triangleq\frac{2\widetilde{Y}[n]-Y[n]}{\widetilde{Y}^2[n]}. \tag{38}$$

It can be observed that all the non-convex constraints have been transformed into convex forms, and we can obtain the optimal trajectory $\{\mathbf{q}_{\text{j}}[n]\}$ and velocity $\{\mathbf{v}_{\text{J}}[n]\}$ of Jack by solving (P5.1).

E. Algorithm for Problem (P1)

Combining the four subproblems discussed above, we propose an iterative algorithm to solve (P1) by applying BCD. We need to select the initial feasible points and obtain the suboptimal solution by solving (P2), (P3.1), (P4.2) and (P5.1) alternatively. The obtained solutions in each iteration are used as the input feasible points for the next iteration.

$$f_6(X[n],\widetilde{X}[n]) \triangleq -\frac{a_k[n]p_{\rm J}[n]\log_2 e(X[n]-\widetilde{X}[n])}{p_{\rm J}^2[n]\widetilde{X}^2[n]+(a_k[n]+2)p_{\rm J}[n]\widetilde{X}[n]+a_k[n]+1}+\log_2\left(1+\frac{a_k[n]}{p_{\rm J}[n]\widetilde{X}[n]+1}\right),\forall k,n. \tag{35}$$

Algorithm 1 Iterative Algorithm for Problem (P1)

Initialization: Set the initial feasible points $\tilde{\mathbf{P}}^0=\{\tilde{p}_k^0[n],\tilde{p}_{\rm J}^0[n]\}$, $\tilde{\mathbf{B}}^0=\{\tilde{\mathbf{q}}_{\rm B}^0[n],\tilde{\mathbf{v}}_{\rm B}^0[n]\}$ and $\tilde{\mathbf{J}}^0=\{\tilde{\mathbf{q}}_{\rm J}^0[n],\tilde{\mathbf{v}}_{\rm J}^0[n]\}$, as well as set the initial values of slack variables $\tilde{H}_k^0[n]$, $\tilde{I}^0[n]$, $\tilde{\lambda}_{\rm B}^0[n]$, $\tilde{X}^0[n]$, $\tilde{Y}^0[n]$, and $\tilde{\lambda}_{\rm J}^0[n]$. $l=0$, $\mathrm{R}(\mathbf{S}^0,\tilde{\mathbf{P}}^0,\tilde{\mathbf{B}}^0,\tilde{\mathbf{J}}^0)=0$.

while $\mathrm{R}(\mathbf{S}^l,\tilde{\mathbf{P}}^l,\tilde{\mathbf{B}}^l,\tilde{\mathbf{J}}^l)-\mathrm{R}(\mathbf{S}^{l-1},\tilde{\mathbf{P}}^{l-1},\tilde{\mathbf{B}}^{l-1},\tilde{\mathbf{J}}^{l-1})\le\epsilon_1$ **do**

1. Solve (P2) for given $\{\tilde{\mathbf{P}}^l,\tilde{\mathbf{B}}^l,\tilde{\mathbf{J}}^l\}$ and obtain the solution $\mathbf{S}^{l+1}$.
2. Solve (P3.1) for given $\{\mathbf{S}^{l+1},\tilde{\mathbf{B}}^l,\tilde{\mathbf{J}}^l\}$ and obtain the solution $\tilde{\mathbf{P}}^{l+1}$.
3. Solve (P4.2) for given $\{\mathbf{S}^{l+1},\tilde{\mathbf{P}}^{l+1},\tilde{\mathbf{J}}^l\}$ and obtain the solution $\tilde{\mathbf{B}}^{l+1}$. Update $\tilde{H}_k^{l+1}[n]$, $\tilde{I}^{l+1}[n]$, and $\tilde{\lambda}_{\rm B}^{l+1}[n]$.
4. Solve (P5.1) for given $\{\mathbf{S}^{l+1},\tilde{\mathbf{P}}^{l+1},\tilde{\mathbf{B}}^{l+1}\}$ and obtain the solution $\tilde{\mathbf{J}}^{l+1}$. Update $\tilde{X}^{l+1}[n]$, $\tilde{Y}^{l+1}[n]$ and $\tilde{\lambda}_{\rm J}^{l+1}[n]$.
5. $l=l+1$.
6. Compute the objective value $\mathrm{R}(\mathbf{S}^l,\tilde{\mathbf{P}}^l,\tilde{\mathbf{B}}^l,\tilde{\mathbf{J}}^l)$.

end

Output: $\mathrm{R}(\mathbf{S}^l,\tilde{\mathbf{P}}^l,\tilde{\mathbf{B}}^l,\tilde{\mathbf{J}}^l)$ with $\mathbf{S}^*=\mathbf{S}^l$, $\mathbf{P}^*=\tilde{\mathbf{P}}^l$, $\mathbf{B}^*=\tilde{\mathbf{B}}^l$, $\mathbf{J}^*=\tilde{\mathbf{J}}^l$.

Define the objective function of the original problem (P1) at the lth iteration as $\mathrm{R}(\mathbf{S}^l,\tilde{\mathbf{P}}^l,\tilde{\mathbf{B}}^l,\tilde{\mathbf{J}}^l)=\sum_{k=1}^K\eta^k$. We summarize the details of overall iterations for (P1) in Algorithm 1.

The convergence of Algorithm 1 is proved as follows.

Proposition 1: Algorithm 1 is convergent.

Proof: In Step 1 of Algorithm 1, we solve a standard linear problem (P2) and obtain the solution $\mathbf{S}^{l+1}$. Thus, we have

$$\mathrm{R}(\mathbf{S}^l,\tilde{\mathbf{P}}^l,\tilde{\mathbf{B}}^l,\tilde{\mathbf{J}}^l)\le\mathrm{R}(\mathbf{S}^{l+1},\tilde{\mathbf{P}}^l,\tilde{\mathbf{B}}^l,\tilde{\mathbf{J}}^l). \tag{39}$$

Then, we obtain the suboptimal solution $\tilde{\mathbf{P}}^{l+1}$ by solving (P3.1), and have

$$\begin{aligned}\mathrm{R}(\mathbf{S}^{l+1},\tilde{\mathbf{P}}^l,\tilde{\mathbf{B}}^l,\tilde{\mathbf{J}}^l)&\overset{(a)}{=}\mathrm{R}^{\rm lb}(\mathbf{S}^{l+1},\tilde{\mathbf{P}}^l,\tilde{\mathbf{B}}^l,\tilde{\mathbf{J}}^l)\\&\overset{(b)}{\le}\mathrm{R}^{\rm lb}(\mathbf{S}^{l+1},\tilde{\mathbf{P}}^{l+1},\tilde{\mathbf{B}}^l,\tilde{\mathbf{J}}^l)\\&\overset{(c)}{\le}\mathrm{R}(\mathbf{S}^{l+1},\tilde{\mathbf{P}}^{l+1},\tilde{\mathbf{B}}^l,\tilde{\mathbf{J}}^l),\end{aligned} \tag{40}$$

where $\mathrm{R}^{\rm lb}(\mathbf{S}^{l+1},\tilde{\mathbf{P}}^{l+1},\tilde{\mathbf{B}}^l,\tilde{\mathbf{J}}^l)=\sum_{k=1}^K\eta_p^k$ is the objective function of the approximate problem (P3.1). The equation (a) holds the fact that the first-order Taylor expansions are tight at the given feasible point; (b) follows that (P3.1) can be solved optimally; (c) holds since the sum ASR of (P3.1) is a lower bound to the objective function of (P1). The inequality (40) demonstrates that the sum ASR is always non-decreasing after each iteration.

The proof of the convergence in Step 3 and Step 4 is similar to that of (40), and the result follows

$$\mathrm{R}(\mathbf{S}^{l+1},\tilde{\mathbf{P}}^{l+1},\tilde{\mathbf{B}}^l,\tilde{\mathbf{J}}^l)\le\mathrm{R}(\mathbf{S}^{l+1},\tilde{\mathbf{P}}^{l+1},\tilde{\mathbf{B}}^{l+1},\tilde{\mathbf{J}}^l), \tag{41}$$

$$\mathrm{R}(\mathbf{S}^{l+1},\tilde{\mathbf{P}}^{l+1},\tilde{\mathbf{B}}^{l+1},\tilde{\mathbf{J}}^l)\le\mathrm{R}(\mathbf{S}^{l+1},\tilde{\mathbf{P}}^{l+1},\tilde{\mathbf{B}}^{l+1},\tilde{\mathbf{J}}^{l+1}). \tag{42}$$

From (39), (40), (41) and (42), we further have

$$\mathrm{R}(\mathbf{S}^l,\tilde{\mathbf{P}}^l,\tilde{\mathbf{B}}^l,\tilde{\mathbf{J}}^l)\le\mathrm{R}(\mathbf{S}^{l+1},\tilde{\mathbf{P}}^{l+1},\tilde{\mathbf{B}}^{l+1},\tilde{\mathbf{J}}^{l+1}), \tag{43}$$

where the inequalities are derived from the non-decreasing property of the optimization problems. Notice that the objective function in (P1) is non-decreasing after each iteration. Owing to the limitation of constraints, the maximum sum ASR is upper bounded by a finite value. Therefore, we can verify that Algorithm 1 is guaranteed to converge to at least a local suboptimal solution to (P1). ■

After the convergence of Algorithm 1, we notice that the node scheduling variables $\tilde{s}_k[n]$ are usually tight and nearly binary ones. Thus, we can discretize $\tilde{s}_k[n]$ into binary ones by comparing with 0.5. The derivation of the computational complexity for Algorithm 1 is similar to that of Algorithm 3 at the end of Section IV.

IV. Optimization for Maximizing SEE

The limited on-board energy significantly influence the flight time and usability of UAVs. Thus, in order to prolong the endurance of UAVs in service, we aim at maximizing the SEE for the secure dual-UAV data collection via jointly optimizing $\mathbf{S}$, $\mathbf{P}$, $\mathbf{B}$ and $\mathbf{J}$.

A. Problem Formulation

The SEE maximization problem can be formulated as

$$(\mathrm{P6}):\max_{\mathbf{S},\mathbf{P},\mathbf{B},\mathbf{J}}\ \mathrm{EE}_{\rm sec} \tag{44a}$$

$$s.t.\ \ \mathrm{C1}-\mathrm{C7},\mathrm{C9}-\mathrm{C13}, \tag{44b}$$

where $\mathrm{EE}_{\rm sec}$ is given by (8). The two problems (P1) and (P6) have most of the same non-convex constraints, and the numerator in $\mathrm{EE}_{\rm sec}$ is the objective function of (P1). Thus, (P6) is a non-convex and mixed integer fractional optimization problem, and the similar SCA method can be adopted to handle these constraints.

B. Proposed Algorithm

Similar to Algorithm 1, we can solve four subproblems iteratively to obtain the suboptimal solutions $\mathbf{S}$, $\mathbf{P}$, $\mathbf{B}$ and $\mathbf{J}$ based on the BCD method. Since only the denominator of the objective function $\mathrm{EE}_{\rm sec}$ is related to the velocity, $\mathbf{S}$ and $\mathbf{P}$ can be obtained by directly solving (P2) and (P3.1), respectively. According to (P6), the optimization problem of $\mathbf{B}$ can be reformulated as

$$(\mathrm{P6.1}):\max_{\mathbf{B},\eta^k}\ \frac{B_wN\sum_{k=1}^K\eta^k}{\sum_{n=1}^N\left(P_{\rm prop}^{\rm B}[n]+P_{\rm prop}^{\rm J}[n]\right)} \tag{45a}$$

$$s.t.\ \ \frac{1}{N}\sum_{n=1}^N\left(s_k[n]\log_2\left(1+\frac{p_k[n]g_{k\rm B}[n]}{p_{\rm J}[n]g_{\rm JB}[n]+\sigma_{\rm B}^2}\right)-\hat{R}_{k\rm E}[n]\right)\ge\eta^k,\forall k, \tag{45b}$$

$$\eta^k\ge R_{\min},\forall k, \tag{45c}$$

$$\mathrm{C9}-\mathrm{C13}, \tag{45d}$$

Algorithm 2 Dinkelbach method for solving (P6.2)

Initialization: Set feasible points $\tilde{\mathbf{B}}^0 = \{\tilde{\mathbf{q}}_{\mathrm{B}}^0[n], \tilde{\mathbf{v}}_{\mathrm{B}}^0[n]\}$. $m = 0$ and $\mu = 0$.

repeat

Solve problem (P6.2) for given $\{\mathbf{S}, \tilde{\mathbf{P}}, \tilde{\mathbf{J}}, \mu\}$ and obtain suboptimal solution $\mathbf{B}^* = \tilde{\mathbf{B}}^{m+1}$.

if $B_w \sum_{k=1}^{K} {\eta_{\mathrm{B}}^k}^*[n] - \frac{1}{N} \sum_{n=1}^{N} \left(f_5(\lambda_{\mathrm{B}}^*[n], \boldsymbol{\nu}_{\mathrm{B}}^*[n]) + P_{\mathrm{prop}}^{\mathrm{J}}[n]\right) \mu \leq \epsilon_2$ **then**

Convergence = **true**.

return $\{\mathbf{B}^*, \mu^*\}$.

else

Update: $m = m + 1$.

$\mu = \mu^* = \frac{B_w \sum_{k=1}^{K} \eta_{\mathrm{B}}^{k\,*}[n]}{\frac{1}{N} \sum_{n=1}^{N} (f_5(\lambda_{\mathrm{B}}^*[n], \mathbf{v}_{\mathrm{B}}^*[n]) + P_{\mathrm{prop}}^{\mathrm{J}}[n])}$.

Convergence = **false**.

end

until *Convergence*;

Algorithm 3 Iterative Algorithm for Problem (P6)

Initialization:Set the initial feasible points $\tilde{\mathbf{P}}^0 = \{\tilde{p}_k^0[n], \tilde{p}_{\mathrm{J}}^0[n]\}$, $\tilde{\mathbf{B}}^0 = \{\tilde{\mathbf{q}}_{\mathrm{B}}^0[n], \tilde{\mathbf{v}}_{\mathrm{B}}^0[n]\}$ and $\tilde{\mathbf{J}}^0 = \{\tilde{\mathbf{q}}_{\mathrm{J}}^0[n], \tilde{\mathbf{v}}_{\mathrm{J}}^0[n]\}$. Set the initial values of slack variables $\tilde{H}_k^0[n]$, $\tilde{I}^0[n]$, $\tilde{\lambda}_{\mathrm{B}}^0[n]$ and $\tilde{X}^0[n]$, $\tilde{Y}^0[n]$, $\tilde{\lambda}_{\mathrm{J}}^0[n]$. $l = 0$ and $\mu^0 = 0$.

while $(\mu^l - \mu^{l-1} \leq \epsilon_2)$ **do**

1. Solve (P2) for given $\{\tilde{\mathbf{P}}^l, \tilde{\mathbf{B}}^l, \tilde{\mathbf{J}}^l\}$ and obtain the solution $\mathbf{S}^{l+1}$.

2. Solve (P3.1) for given $\{\mathbf{S}^{l+1}, \tilde{\mathbf{B}}^l, \tilde{\mathbf{J}}^l\}$ and obtain the solution $\tilde{\mathbf{P}}^{l+1}$.

3. Solve (P4.3) via Algorithm 2 and obtain the suboptimal result $\{\tilde{\mathbf{B}}^{l+1}\}$.

4. Obtain the suboptimal result $\{\tilde{\mathbf{J}}^{l+1}\}$ via Algorithm 2.

5. Update: $l = l + 1$.

6. Compute objective value of (P6) μ^l.

end

Output: μ^l with $\mathbf{S}^* = \mathbf{S}^l$, $\mathbf{P}^* = \tilde{\mathbf{P}}^l$, $\mathbf{B}^* = \tilde{\mathbf{B}}^l$, and $\mathbf{J}^* = \tilde{\mathbf{J}}^l$.

where η^k is defined in (13). We can adopt the Dinkelbach method to solve the fractional programming problem (P6.1) iteratively [42]. Define $\mu \in \mathbb{R}$ as the SEE, and the objective function can be transformed from a fractional expression into an integral one. According to the similar transformation in Section III-C, (P6.1) can be approximated as

$$(\mathrm{P6.2}): \max_{\substack{\mathbf{B}, \eta_{\mathrm{B}}^k, \lambda_{\mathrm{B}}[n], \\ H_k[n], I[n], D[n]}} \tilde{\Phi}(\mu) \tag{46a}$$

$$s.t. \ \ (31\mathrm{b}) - (31\mathrm{e}), (31\mathrm{g}), \tag{46b}$$

where

$$\tilde{\Phi}(\mu) = B_w N \sum_{k=1}^{K} \eta_{\mathrm{B}}^k - \sum_{n=1}^{N} \left(f_5(\lambda_{\mathrm{B}}[n], \mathbf{v}_{\mathrm{B}}[n]) + P_{\mathrm{prop}}^{\mathrm{J}}[n]\right) \mu, \tag{47}$$

where $f_5(\lambda_{\mathrm{B}}[n], \mathbf{v}_{\mathrm{B}}[n])$ is defined in (32).

In addition, we define μ^* and $\{\mathbf{q}_{\mathrm{B}}^*, \mathbf{v}_{\mathrm{B}}^*\}$ as the maximum secrecy energy efficiency and the suboptimal solution to (P6.2), respectively. Thus, we have the following theorem.

TABLE I
SIMULATION PARAMETERS

Parameter	Simulation Value	Parameter	Simulation Value
ρ_0	-60 dB	Ω	300 rad/s
σ_{B}^2, σ_{E}^2	-110 dBm	r	0.4 m
B_w	1 MHz	ρ	1.225 kg/m^3
$\tilde{D}$	15 m	s	0.05
H	150 m	A	0.503 m^2
K	3	v_0	4.03 m/s
$\mathbf{q}_{\mathrm{B},I}$,$\mathbf{q}_{\mathrm{B},F}$	$[600, 600]^T$ m	d_0	0.6
$\mathbf{q}_{\mathrm{J},I}$,$\mathbf{q}_{\mathrm{J},F}$	$[600, 500]^T$ m	P_0	79.86 W
$\tilde{\mathbf{w}}_{\mathrm{E}}$	$[500, 500]^T$ m	P_i	88.63 W
$\mathbf{w}_k$	$[1000, 1000]^T$, $[200, 600]^T$, $[900, 150]^T$ m	$V_{\max}$	30 m/s , 3 m/s^2
$P_{\mathrm{ave}}^{\mathrm{J}}$	10 dBm	$a_{\max}$	
$P_{\max}^{\mathrm{J}}$	16 dBm	δ_t	1 s
ϵ_1, ϵ_2	10^{-3}	$R_{\min}$	2 bit/s/Hz
		α	3

Theorem 1: If and only if there exists an optimal parameter μ^* for (P6.2), we have $\tilde{\Phi}(\mu^*) = 0$.

Proof: Define $h(\mathbf{q}_{\mathrm{B}}) = B_w N \sum_{k=1}^{K} \eta_{\mathrm{B}}^k$ and $g(\mathbf{v}_{\mathrm{B}}) = \sum_{n=1}^{N} \left(f_5(\lambda_{\mathrm{B}}[n], \mathbf{v}_{\mathrm{B}}[n]) + P_{\mathrm{prop}}^{\mathrm{J}}[n]\right)$, and we have $\frac{h(\mathbf{q}_{\mathrm{B}}^*)}{g(\mathbf{v}_{\mathrm{B}}^*)} = \mu^* \Rightarrow h(\mathbf{q}_{\mathrm{B}}^*) - g(\mathbf{v}_{\mathrm{B}}^*)\mu^* = 0$. Let $\{\mathbf{q}_b, \mathbf{v}_{\mathrm{B}}\} \neq \{\mathbf{q}_{\mathrm{B}}^*, \mathbf{v}_{\mathrm{B}}^*\}$ be the arbitrary feasible solution to (P6.2), and we can know that there exists $\frac{h(\mathbf{q}_{\mathrm{B}})}{g(\mathbf{v}_{\mathrm{B}})} \leq \mu^* \Rightarrow h(\mathbf{q}_{\mathrm{B}}) - g(\mathbf{v}_{\mathrm{B}})\mu^* \leq 0$. Thus, we have

$$\max_{\mathbf{q}_{\mathrm{B}}, \mathbf{v}_{\mathrm{B}}} \ \ h(\mathbf{q}_{\mathrm{B}}) - g(\mathbf{v}_{\mathrm{B}})\mu^* = 0, \tag{48}$$

which is achievable by the suboptimal solution $\{\mathbf{q}_{\mathrm{B}}^*, \mathbf{v}_{\mathrm{B}}^*\}$. ■

The Dinkelbach method is summarized in Algorithm 2. In the algorithm, the objective function of the fractional programming is first transformed into an equivalent parametric optimization problem, and then ϵ-optimal solutions are obtained iteratively, where ϵ_2 is the tolerance of convergence. Thus, we can obtain the suboptimal solution $\mathbf{B}^*$ via Algorithm 2. Then, we notice that the optimization of $\mathbf{J}$ is also a fractional programming problem, which can be reformulated according to (P6). This subproblem can be similarly solved by the Dinkelbach method via Algorithm 2.

Finally, the original problem (P6) can be efficiently solved through the BCD method and the overall steps are summarized in Algorithm 3. The convergence and the local optimality of Algorithm 3 can be verified in a similar way to Algorithm 1, which are omitted to make the paper compact.

In Algorithm 3, (P2) is a standard linear programming, which can be solved by the interior point method with the complexity $\mathcal{O}(\sqrt{KN + K} \log \frac{1}{\epsilon_0})$, where $KN + K$ denotes the total number of variables and ϵ_0 is the accuracy of SCA for solving (P2). Since (P3.1) involves the logarithmic form, the complexity is $\mathcal{O}((KN + K + N)^{3.5} \log \frac{1}{\epsilon_0})$ according to [27]. Note that Step 3 includes a inner loop, and its complexity can be expressed as $\mathcal{O}(L_1((KN + K + 7N)^{3.5} \log \frac{1}{\epsilon_0}))$, where L_1 denotes the iteration number for updating μ in Algorithm 2. Similar to (P6.2), the complexity of the last subproblem in Step 4 is $\mathcal{O}(L_2((K + 7N)^{3.5} \log \frac{1}{\epsilon_0}))$. According to the above analysis, we can derive the computational complexity of Algorithm 3 in (49) at the top of the page.

V. SIMULATION RESULTS AND ANALYSIS

In this section, we provide numerical simulation results to evaluate the effectiveness of the proposed schemes. The peak

$$\mathcal{O}\left(M_1\left(\sqrt{KN+K}\log\frac{1}{\epsilon_0}+(KN+K+N)^{3.5}\log\frac{1}{\epsilon_0}+L_1\left((KN+K+7N)^{3.5}\log\frac{1}{\epsilon_0}\right)+L_2\left((K+7N)^{3.5}\log\frac{1}{\epsilon_0}\right)\right)\right), \quad (49)$$

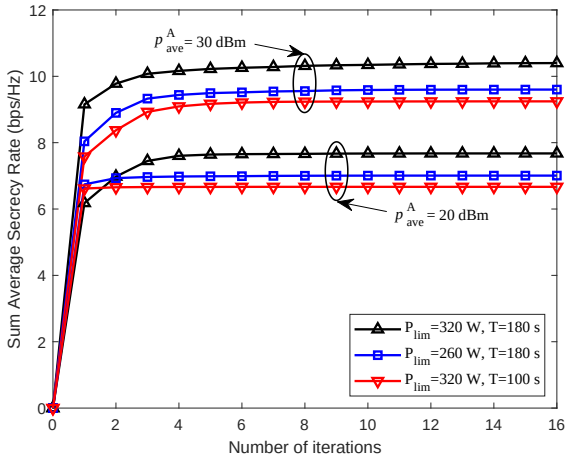

Fig. 2. The average secrecy rate versus the number of iterations.

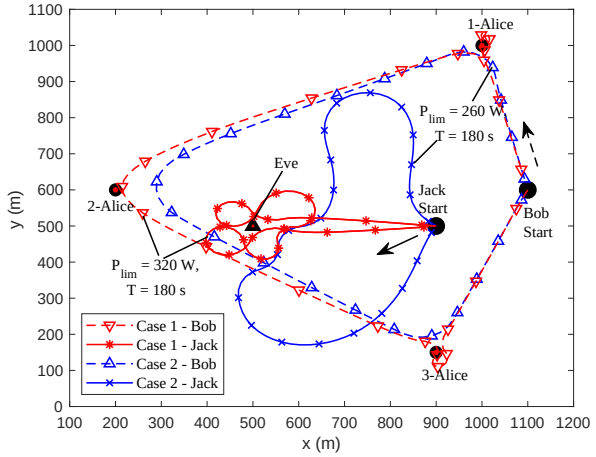

(a) Optimized trajectories of Bob and Jack for different propulsion power limit $P_{\lim}$ with T = 180 s.

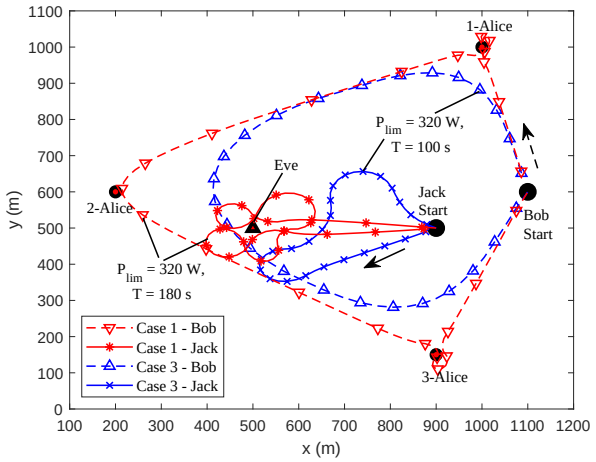

(b) Optimized trajectories of Bob and Jack for different T with $P_{\lim}$ = 320 W.

Fig. 3. Optimized UAVs' trajectories for the ASR-LP scheme in different scenarios.

transmit power is set as $P^{\mathrm{A}}_{\max} = 4P^{\mathrm{A}}_{\mathrm{ave}}$. Simulation parameters are summarized in Table I.

In order to show the superiority of the proposed schemes in terms of sum ASR and SEE, we consider the following benchmark schemes.

- **ASR-LP scheme:** The proposed scheme of Algorithm 1, aiming to maximize the sum ASR with limited propulsion power via jointly optimizing $\mathbf{S}$, $\mathbf{P}$, $\mathbf{B}$ and $\mathbf{J}$.
- **SEE scheme:** The proposed scheme of Algorithm 3 in maximize the SEE via jointly optimizing $\mathbf{S}$, $\mathbf{P}$, $\mathbf{B}$ and $\mathbf{J}$.
- **ASR-NLP scheme:** The sum ASR is maximized without propulsion power limitation, i.e., without C8.
- **ASR-LP-NPC scheme:** The ASR-LP scheme without optimizing the transmit power $\mathbf{P}$, which is equally set over time, i.e., $p_k[n] = P^{\mathrm{A}}_{\mathrm{ave}}$ and $p_{\mathrm{J}}[n] = P^{\mathrm{J}}_{\mathrm{ave}}, \forall n, k$.

A. Initialization and Convergence of Algorithm 1

Since iteration is adopted in **Algorithm 1** and **Algorithm 3**, the initialization of UAVs' trajectories has a great influence on the convergence and performance of the schemes. The initial flight trajectory of each UAV is assumed to be a circular at constant speed, whose center is the geometric center of ground nodes, i.e., $\mathbf{C} = \sum_{k=1}^{K} \mathbf{w}_k/K$. It is suitable for the UAV Bob to visit all nodes, and its initial flight radius can be computed according to $\mathbf{R}_{\mathrm{B}} = \min(\frac{V_{\max}T}{2\pi}, \|\mathbf{C} - \mathbf{w}_k\|)$. The UAV Jack should stay around Eve to disrupt the eavesdropping, and its initial flight radius is defined as $\mathbf{R}_{\mathrm{J}} = \mathbf{R}_{\mathrm{B}}/2$. The initial velocity $\mathbf{v}_i[n]$ can be simply obtained according to $\mathbf{v}_i[n] = (\mathbf{q}_i[n+1] - \mathbf{q}_i[n])/\delta_t, \forall i \in \{\mathrm{B}, \mathrm{J}\}$. Based on initial flight trajectories, the initial jamming power $\tilde{p}^0_{\mathrm{J}}[n]$ is set as $\tilde{p}^0_{\mathrm{J}}[n] = P^{\mathrm{J}}_{\mathrm{ave}}$. The initial transmit power is set as $\tilde{p}^0_k[n] = P^{\mathrm{A}}_{\mathrm{ave}}$ if $R_{k\mathrm{B}}[n] - \hat{R}_{k\mathrm{E}}[n]$ is non-negative, and $\tilde{p}^0_k[n] = 0$ otherwise.

We first present the convergence of Algorithm 1 in Fig. 2 for different T, $P_{\lim}$ and $P^{\mathrm{A}}_{\mathrm{ave}}$. It can be observed that a higher transmit power can be used to improve the secure performance, and these cases of $P^{\mathrm{A}}_{\mathrm{ave}}$ = 20 dBm converge a little faster than $P^{\mathrm{A}}_{\mathrm{ave}}$ = 30 dBm. Moreover, the sum ASR becomes higher for a larger T and $P_{\lim}$, due to more resources utilized. Algorithm 1 converges quickly within 5 iterations for all the cases.

B. Simulation Results of ASR-LP Scheme

Fig. 3 illustrates the optimized UAVs' trajectories for the ASR-LP scheme. Notice that the black arrows denote the flight directions of the two UAVs, which are towards opposite

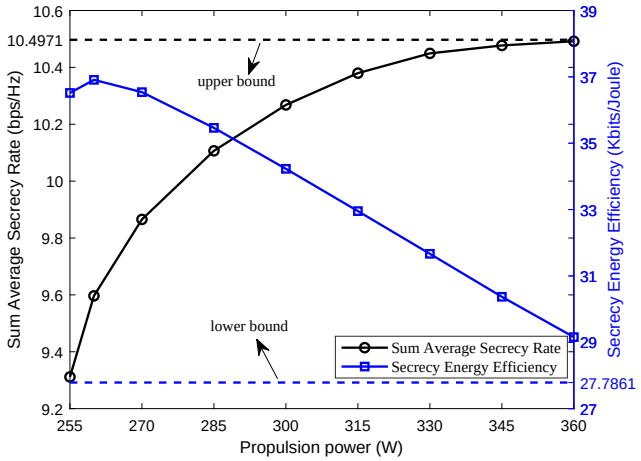

Fig. 4. Sum average secrecy rate and secrecy energy efficiency against $P_{\lim}$ in the ASR-LP scheme when T = 180 s.

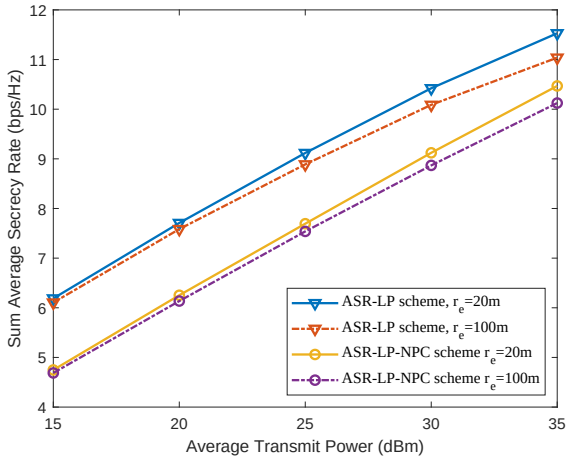

Fig. 5. Performance comparison of the ASR-LP scheme and the ASR-LP-NPC scheme.

directions. This is mainly due to the fact that Bob can also receive the noise-like interference from Jack, and Jack should be careful not to move too close to Bob when it flies towards the eavesdropper. In order to analyze the influence of the flight time T and the average propulsion power budget $P_{\lim}$, we consider three cases: 1) T = 180 s, $P_{\lim}$ = 320 W; 2) T = 180 s, $P_{\lim}$ = 260 W; 3) T = 100 s, $P_{\lim}$ = 320 W. In Fig. 3(a), we plot the optimized trajectories of Case 1 and Case 2. For Case 2 with $P_{\lim}$ = 260 W, the trajectory of Jack has a larger turning radius, which demonstrates that the propulsion power is lower with the smooth path and the steady speed. However, when $P_{\lim}$ becomes higher, Bob and Jack can move faster to ground nodes and eavesdropper, respectively. The smaller turning radius of trajectory can help UAV hover or turn around more flexibly, which can effectively enhance the performance. Fig. 3(b) shows the optimized UAVs' trajectories with different T when $P_{\lim}$ = 320 W. For Case 3 with T = 100 s, Bob attempts to approach all ground nodes but it is unable to fly over them due to the limitation of T. As T increases, Bob can adjust its trajectory to visit all nodes, which can significantly improve the channel conditions. However, even if T is sufficiently large, the UAVs cannot stay stationary above the nodes for a long time due to the limitation of propulsion power.

Fig. 4 shows the sum ASR and SEE versus $P_{\lim}$ in the ASR-LP scheme when T = 180 s, and the two dotted lines denote the upper bound of sum ASR and the lower bound of SEE for the ASR-NLP scheme, respectively. These two bounds are both calculated with $P_{\lim} \to \infty$, and the ASR-LP scheme changes into the ASR-NLP scheme in this case. In this figure, we first observe that the sum ASR increases with $P_{\lim}$. This is due to the fact that higher $P_{\lim}$ provides more degrees of freedom for the trajectory and velocity. In addition, we observe that the SEE first increases, and then monotonically decreases. This is because the incrementation of the sum ASR is first larger than the incrementation of propulsion power consumption when $P_{\lim}$ is small. In contrast, the sum ASR growth slows down with the increase of $P_{\lim}$, and thus the SEE then decreases.

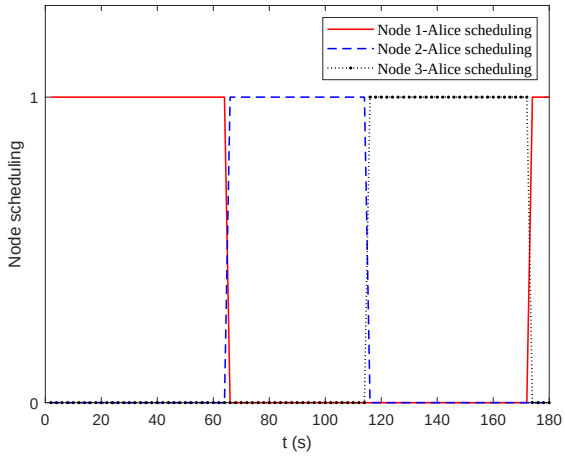

Fig. 6. The node scheduling for the SEE scheme with period T = 180 s.

In Fig. 5, we compare the performance between the ASR-LP scheme and ASR-LP-NPC scheme with different average transmit power when T = 180 s, $P_{\lim}$ = 320 W and $R_{\min}$ = 1 bit/s/Hz. It is clear that the power control can improve the performance effectively. Furthermore, as the average transmit power increases, the gaps of the ASR between the two schemes decrease. This is because the trajectories of Bob are similar, and the rate gain provided by the power control decreases as the transmit power increases. In addition, the uncertain region parameter r_e also affects the performance, and a larger r_e will cause more threat from the eavesdropper on the secure transmission.

C. Simulation Results of SEE Scheme

To explicitly describe the optimization result of the SEE scheme, the optimized scheduling and transmit power are plotted in Fig. 6 and Fig. 7, respectively. We can observe from Fig. 6 that these nodes are woken up alternately, which indicates that while one node is working, the others keep silence. Fig. 7 shows that the node near the eavesdropper has

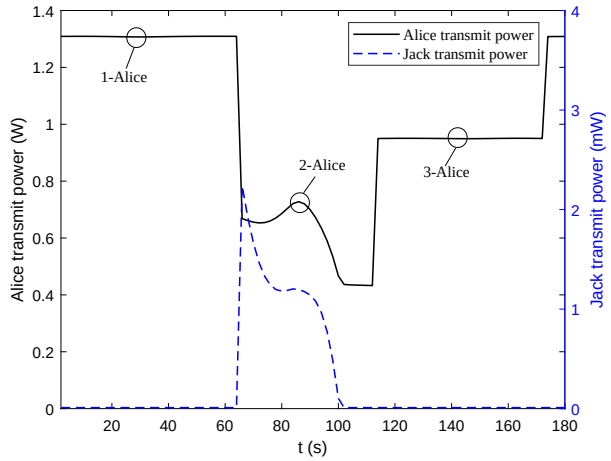

Fig. 7. The transmit power allocation for SEE scheme with period T = 180 s.

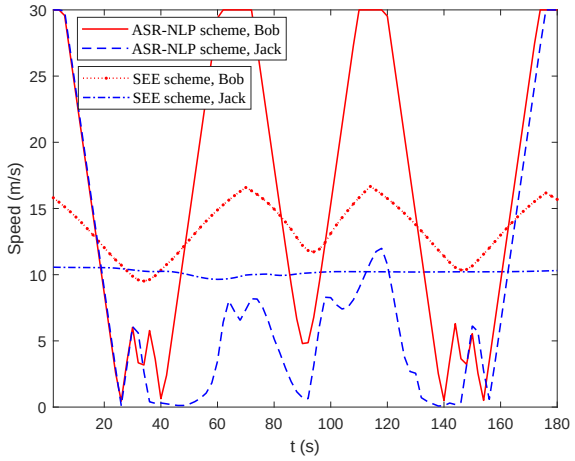

Fig. 9. The speeds of UAVs for the ASR-NLP scheme and the SEE scheme with T = 180 s.

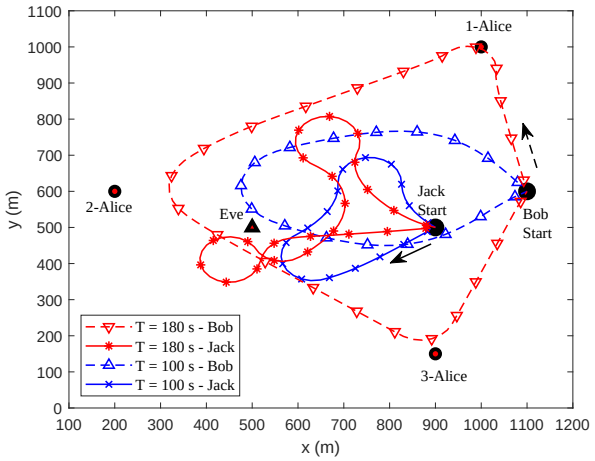

Fig. 8. Optimized secrecy energy efficient UAVs' trajectories for different T.

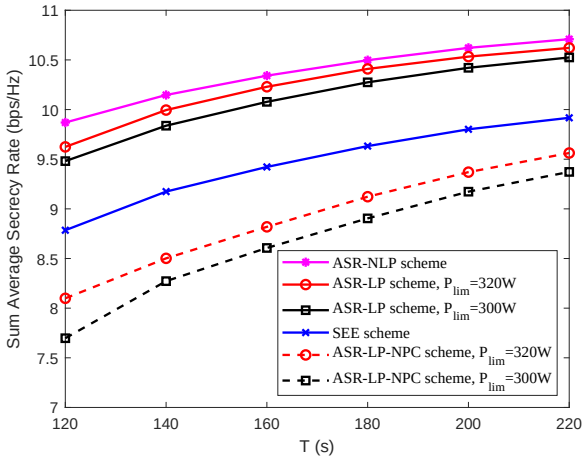

Fig. 10. The average secrecy rate with respect to the period T.

a lower transmit power level to weaken the wiretap channel. Specifically, as the UAV moves closer to 2-Alice, the transmit power increases from t = 66 s to t = 86 s, while as the UAV is far away from 2-Alice, the transmit power decreases from t = 86 s to t = 114 s. In addition, Jack transmits artificial noise only when 2-Alice is transmitting, because it is much closer to Eve than the other two ground sensors. When the distance from each sensor to Eve does not differ much, Jack will transmit artificial noise all the time.

Then, we present the optimized trajectories of SEE scheme with different T in Fig. 8. When T = 100 s, the UAVs simply fly in a small circular region due to the limitation of flight period. In contrast, when T is 180 s, Bob prefers to move closer to the ground nodes and farther away from the eavesdropper to enhance the sum ASR. Meanwhile, Bob maintains flying around the legitimate ground nodes with an appropriate speed, instead of staying stationary above them. This can be expected since with an appropriate speed, the energy consumption of the rotary-wing UAVs is lower. Thus, the SEE scheme can provide a tradeoff between the sum ASR and the cost of energy. In order to demonstrate the performance of the SEE scheme, we plot Fig. 9 to show the UAV speed with T = 180 s. For comparison, we also consider the ASR-NLP scheme. We can observe that Bob flies with the maximum speed $V_{\max}$ between ground nodes and hovers above each of them with a much lower speed for the ASR-NLP scheme. This can be expected since for the sum ASR is maximized without considering the UAV's energy consumption, and it is preferable for Bob to fly to the ground nodes as soon as possible to improve the transmission quality. On the other hand, the proposed SEE scheme holds the speed of the UAV at around 10 m/s in order to achieve a balance between maximizing the secrecy rate and minimizing the propulsion power consumption.

D. Comparison of Proposed Schemes with Benchmarks

Finally, Fig. 10 and Fig. 11 illustrate the sum ASR and the SEE comparison of these schemes with different T, respectively. It can be observed that the sum ASR and the SEE of all the schemes increase significantly with T. The

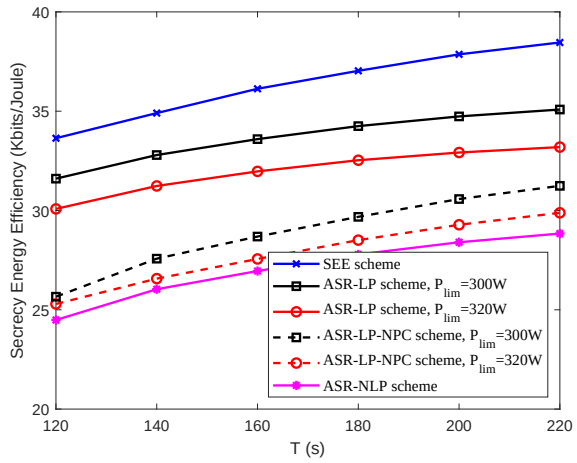

Fig. 11. The secrecy energy efficiency with respect to the period T.

reason is that as the total flight time increases, the UAVs have more time to hover over the desirable points to achieve a more efficient transmission. Although the ASR-NLP scheme has an excellent performance on the sum ASR, the SEE performance is the worst compared with the other schemes. If the power budget of UAVs is predefined, the ASR-LP scheme can take full advantage of the finite energy to design the trajectories and other parameters, and thus the sum ASR and the SEE will maintain in a high level. Furthermore, the SEE scheme can achieve a goal that strikes an optimal balance between the sum ASR and energy consumption, through which the SEE can be maximized with the acceptable sum ASR.

VI. Conclusions

In this paper, we jointly design the resource allocation including the scheduling, the transmit power, and the trajectory and velocity of UAVs, aiming to maximize the sum ASR and SEE of a secure dual-UAV communication system, respectively. The joint design of maximizing the sum ASR is formulated as a non-convex optimization problem by taking into account the limitation of UAV average propulsion power. An efficient iterative algorithm based on BCD and SCA is proposed to achieve a suboptimal solution. Then, we consider to maximize the SEE, which can be formulated as a fractional and mixed integer nonlinear programming problem. The Dinkelbach method can be applied to transform the fractional optimization problem into an equivalent parametric one, and then we propose an iterative algorithm to obtain a suboptimal solution. Simulation results show that the appropriate parameters can be designed to optimize the ASR or SEE performance according to the UAV battery capacity and the flight time via the proposed schemes.

Appendix A
Proof of Lemma 1

According to the Jensen's inequality, if $f(x)$ is concave with respect to x, we have

$$\mathbb{E}_x(f(x)) \leq f(\mathbb{E}_x(x)). \tag{50}$$

Note that $\log_2\left(1+\frac{\frac{p_k[n]\rho_0}{\|\mathbf{w}_k-\mathbf{w}_\mathrm{E}\|^\alpha}\zeta}{p_\mathrm{J}[n]g_\mathrm{JE}[n]+\sigma_\mathrm{E}^2}\right)$ is concave with respect to ζ, and we have

$$\begin{aligned} R_{k\mathrm{E}}[n] &= s_k[n]\mathbb{E}_\zeta\left[\log_2\left(1+\frac{\frac{p_k[n]\rho_0}{\|\mathbf{w}_k-\mathbf{w}_\mathrm{E}\|^\alpha}\zeta}{p_\mathrm{J}[n]g_\mathrm{JE}[n]+\sigma_\mathrm{E}^2}\right)\right] \\ &\leq s_k[n]\log_2\left(1+\frac{\frac{p_k[n]\rho_0}{\|\mathbf{w}_k-\mathbf{w}_\mathrm{E}\|^\alpha}\mathbb{E}_\zeta[\zeta]}{p_\mathrm{J}[n]g_\mathrm{JE}[n]+\sigma_\mathrm{E}^2}\right) \\ &= s_k[n]\log_2\left(1+\frac{\frac{p_k[n]\rho_0}{\|\mathbf{w}_k-\mathbf{w}_\mathrm{E}\|^\alpha}}{p_\mathrm{J}[n]g_\mathrm{JE}[n]+\sigma_\mathrm{E}^2}\right). \end{aligned} \tag{51}$$

According to the previous assumption $\|\mathbf{w}_k-\tilde{\mathbf{w}}_\mathrm{E}\|\geq r_\mathrm{E}$, we need to eliminate the uncertainty of Eve by applying the triangular inequality and the inverse triangular inequality as

$$\begin{aligned} \|\mathbf{q}_\mathrm{J}[n]-\mathbf{w}_\mathrm{E}\| &\leq \|\mathbf{q}_\mathrm{J}[n]-\tilde{\mathbf{w}}_\mathrm{E}\|+\|\tilde{\mathbf{w}}_\mathrm{E}-\mathbf{w}_\mathrm{E}\| \\ &\leq \|\mathbf{q}_\mathrm{J}[n]-\tilde{\mathbf{w}}_\mathrm{E}\|+r_\mathrm{E}, \end{aligned} \tag{52}$$

and

$$\begin{aligned} \|\mathbf{w}_k-\mathbf{w}_\mathrm{E}\| &\geq \big|\|\mathbf{w}_k-\tilde{\mathbf{w}}_\mathrm{E}\|-\|\tilde{\mathbf{w}}_\mathrm{E}-\mathbf{w}_\mathrm{E}\|\big| \\ &\geq \big|\|\mathbf{w}_k-\tilde{\mathbf{w}}_\mathrm{E}\|-r_\mathrm{E}\big|. \end{aligned} \tag{53}$$

With (52) and (53), (51) can be written as (10).

Appendix B
Proof of Lemma 2

Define a bivariate function $f(x_1,x_2)\triangleq\log_2(1+\frac{1}{x_1x_2})$, where $x_1>0$ and $x_2>0$. The Hessian matrix of $f(x_1,x_2)$ can be given by

$$\begin{aligned} \nabla^2 f(x_1,x_2) &= \frac{\log_2 e}{(x_1x_2+1)^2}\begin{bmatrix}\frac{2x_2}{x_1}+\frac{1}{x_1^2} & 1\\ 1 & \frac{2x_1}{x_2}+\frac{1}{x_2^2}\end{bmatrix} \\ &= \frac{\log_2 e}{x_1x_2+1}\begin{bmatrix}\frac{1}{x_1^2} & 0\\ 0 & \frac{1}{x_2^2}\end{bmatrix}+\frac{\log_2 e}{(x_1x_2+1)^2}\begin{bmatrix}\sqrt{\frac{x_2}{x_1}}\\ \sqrt{\frac{x_1}{x_2}}\end{bmatrix}\begin{bmatrix}\sqrt{\frac{x_2}{x_1}} & \sqrt{\frac{x_1}{x_2}}\end{bmatrix}\succeq\mathbf{0}. \end{aligned} \tag{54}$$

Note that $f(x_1,x_2)$ is convex with respect to x_1 and x_2. Thus, the first-order Taylor expansion of $f(x_1,x_2)$ at the given feasible point $(\widetilde{x}_1,\widetilde{x}_2)$ can be expressed as

$$f(x_1,x_2)\geq f(\widetilde{x}_1,\widetilde{x}_2)-\frac{\log_2 e(x_1-\widetilde{x}_1)}{\widetilde{x}_1^2\widetilde{x}_2+\widetilde{x}_1}-\frac{\log_2 e(x_2-\widetilde{x}_2)}{\widetilde{x}_2^2\widetilde{x}_1+\widetilde{x}_2}. \tag{55}$$

As the left-hand-side of (21b) is jointly convex with respect to $H_k[n]$ and $I[n]$, we substitute variables $H_k[n]$, $I[n]$, $\widetilde{H}_k[n]$ and $\widetilde{I}[n]$ into (55) and the inequality (22) can be obtained.

Appendix C
Proof of Lemma 3

Define the function $f(x;a,b)=\log_2(1+\frac{a}{bx+1})$ with $a,b\geq 0$, and the first and second order derivatives of $f(x)$ can be given by

$$\nabla f(x) = -\frac{\log_2 eab}{b^2x^2+(a+2)bx+a+1}, \tag{56}$$

$$\nabla^2 f(x)\geq 0. \tag{57}$$

Note that $f(x)$ is a convex function with respect to x when $a, b \geq 0$. Therefore, its first Taylor expansion providing a lower bound at the given point $\widetilde{x}$ can be expressed as

$$f(x) \geq f(\widetilde{x}) - \frac{\log_2 eab}{b^2\widetilde{x}^2 + (a+2)b\widetilde{x} + a + 1}(x - \widetilde{x}). \quad (58)$$

The terms $\log_2\left(1 + \frac{a_k[n]}{p_J[n]X[n]+1}\right)$ in the left-hand-side of (33b) follow (57), which are convex with respect to $X[n]$. According to the inequality (58), we can obtain (34).

REFERENCES

[1] R. Zhang, X. Pang, W. Lu, N. Zhao, M. Liu, Y. Chen, and D. Niyato, "Cooperative UAV-assisted secure uplink communications with propulsion power limitation," in *Proc. IEEE ICC'21*. Montreal, Canada, Jun. 2021, pp. 1–6.

[2] K. P. Valavanis and G. J. Vachtsevanos, *Handbook of Unmanned Aerial Vehicles*. Springer Netherlands, 2015.

[3] Y. Zeng, Q. Wu, and R. Zhang, "Accessing from the sky: A tutorial on UAV communications for 5G and beyond," *Proc. IEEE*, vol. 107, no. 12, pp. 2327–2375, Dec. 2019.

[4] N. Zhao, W. Lu, M. Sheng, Y. Chen, J. Tang, F. R. Yu, and K. Wong, "UAV-assisted emergency networks in disasters," *IEEE Wireless Commun.*, vol. 26, no. 1, pp. 45–51, Feb. 2019.

[5] M. Liu, J. Yang, and G. Gui, "DSF-NOMA: UAV-assisted emergency communication technology in a heterogeneous internet of things," *IEEE Internet Things J.*, vol. 6, no. 3, pp. 5508–5519, Jun. 2019.

[6] R. Fan, J. Cui, S. Jin, K. Yang, and J. An, "Optimal node placement and resource allocation for UAV relaying network," *IEEE Commun. Lett.*, vol. 22, no. 4, pp. 808–811, Apr. 2018.

[7] Y. Zeng, R. Zhang, and T. J. Lim, "Throughput maximization for UAV-enabled mobile relaying systems," *IEEE Trans. Commun.*, vol. 64, no. 12, pp. 4983–4996, Dec. 2016.

[8] A. Al-Hourani, S. Kandeepan, and S. Lardner, "Optimal LAP altitude for maximum coverage," *IEEE Wireless Commun. Lett.*, vol. 3, no. 6, pp. 569–572, Dec. 2014.

[9] M. Mozaffari, W. Saad, M. Bennis, and M. Debbah, "Unmanned aerial vehicle with underlaid device-to-device communications: Performance and tradeoffs," *IEEE Trans. Wireless Commun.*, vol. 15, no. 6, pp. 3949–3963, Jun. 2016.

[10] J. Lyu and R. Zhang, "Network-connected UAV: 3-D system modeling and coverage performance analysis," *IEEE Internet Things J.*, vol. 6, no. 4, pp. 7048–7060, Aug. 2019.

[11] J. Lyu, Y. Zeng, and R. Zhang, "Cyclical multiple access in UAV-aided communications: A throughput-delay tradeoff," *IEEE Wireless Commun. Lett.*, vol. 5, no. 6, pp. 600–603, Dec. 2016.

[12] Q. Wu, Y. Zeng, and R. Zhang, "Joint trajectory and communication design for multi-UAV enabled wireless networks," *IEEE Trans. Wireless Commun.*, vol. 17, no. 3, pp. 2109–2121, Mar. 2018.

[13] C. Shen, T. Chang, J. Gong, Y. Zeng, and R. Zhang, "Multi-UAV interference coordination via joint trajectory and power control," *IEEE Trans. Signal Process.*, vol. 68, pp. 843–858, Jan. 2020.

[14] Y. Zeng, J. Xu, and R. Zhang, "Energy minimization for wireless communication with rotary-wing UAV," *IEEE Trans. Wireless Commun.*, vol. 18, no. 4, pp. 2329–2345, Apr. 2019.

[15] Y. Zeng and R. Zhang, "Energy-efficient UAV communication with trajectory optimization," *IEEE Trans. Wireless Commun.*, vol. 16, no. 6, pp. 3747–3760, Jun. 2017.

[16] C. Zhan and H. Lai, "Energy minimization in internet-of-things system based on rotary-wing UAV," *IEEE Wireless Commun. Lett.*, vol. 8, no. 5, pp. 1341–1344, Oct. 2019.

[17] T. Zhang, Y. Xu, J. Loo, D. Yang, and L. Xiao, "Joint computation and communication design for UAV-assisted mobile edge computing in IoT," *IEEE Trans. Ind. Informat.*, vol. 16, no. 8, pp. 5505–5516, Apr. 2020.

[18] X. Pang, J. Tang, N. Zhao, X. Y. Zhang, and Y. Qian, "Energy-efficient design for mmwave-enabled NOMA-UAV networks," *Sci. China Inf. Sci.*, Aug. 2020. [Online]. Available: https://engine.scichina.com/doi/10.1007/s11432-020-2985-8

[19] E. Turgut, M. Cenk Gursoy, and I. Guvenc, "Energy harvesting in unmanned aerial vehicle networks with 3D antenna radiation patterns," *IEEE Trans. Green Commun. and Netw.*, vol. 4, no. 4, pp. 1149–1164, Dec. 2020.

[20] S. Eom, H. Lee, J. Park, and I. Lee, "UAV-aided wireless communication designs with propulsion energy limitations," *IEEE Trans. Veh. Technol.*, vol. 69, no. 1, pp. 651–662, Jan. 2020.

[21] J. Zhang, Y. Zeng, and R. Zhang, "Receding horizon optimization for energy-efficient UAV communication," *IEEE Wireless Commun. Lett.*, vol. 9, no. 4, pp. 490–494, Apr. 2020.

[22] S. Ahmed, M. Z. Chowdhury, and Y. M. Jang, "Energy-efficient UAV relaying communications to serve ground nodes," *IEEE Wireless Commun. Lett.*, vol. 24, no. 4, pp. 849–852, Apr. 2020.

[23] S. Say, H. Inata, J. Liu, and S. Shimamoto, "Priority-based data gathering framework in UAV-assisted wireless sensor networks," *IEEE Sensors J.*, vol. 16, no. 14, pp. 5785–5794, Jul. 2016.

[24] C. Zhan, Y. Zeng, and R. Zhang, "Energy-efficient data collection in UAV enabled wireless sensor network," *IEEE Wireless Commun. Lett.*, vol. 7, no. 3, pp. 328–331, Jun. 2018.

[25] C. Zhan and Y. Zeng, "Aerial-ground cost tradeoff for multi-UAV-enabled data collection in wireless sensor networks," *IEEE Trans. Commun.*, vol. 68, no. 3, pp. 1937–1950, Mar. 2020.

[26] D. He, S. Chan, and M. Guizani, "Communication security of unmanned aerial vehicles," *IEEE Wireless Commun.*, vol. 24, no. 4, pp. 134–139, Aug. 2017.

[27] G. Zhang, Q. Wu, M. Cui, and R. Zhang, "Securing UAV communications via joint trajectory and power control," *IEEE Trans. Wireless Commun.*, vol. 18, no. 2, pp. 1376–1389, Feb. 2019.

[28] M. Cui, G. Zhang, Q. Wu, and D. W. K. Ng, "Robust trajectory and transmit power design for secure UAV communications," *IEEE Trans. Veh. Technol.*, vol. 67, no. 9, pp. 9042–9046, Sep. 2018.

[29] C. O. Nnamani, M. R. A. Khandaker, and M. Sellathurai, "UAV-aided jamming for secure ground communication with unknown eavesdropper location," *IEEE Access*, vol. 8, pp. 72 881–72 892, Apr. 2020.

[30] A. Li, Q. Wu, and R. Zhang, "UAV-enabled cooperative jamming for improving secrecy of ground wiretap channel," *IEEE Wireless Commun. Lett.*, vol. 8, no. 1, pp. 181–184, Feb. 2019.

[31] Y. Cai, F. Cui, Q. Shi, M. Zhao, and G. Y. Li, "Dual-UAV-enabled secure communications: Joint trajectory design and user scheduling," *IEEE J. Sel. Areas Commun.*, vol. 36, no. 9, pp. 1972–1985, Sep. 2018.

[32] M. T. Mamaghani and Y. Hong, "Improving PHY-security of UAV-enabled transmission with wireless energy harvesting: Robust trajectory design and communications resource allocation," *IEEE Trans. Veh. Technol.*, vol. 69, no. 8, pp. 8586–8600, Aug. 2020.

[33] W. Wang, J. Tang, N. Zhao, X. Liu, X. Y. Zhang, Y. Chen, and Y. Qian, "Joint precoding optimization for secure SWIPT in UAV-aided NOMA networks," *IEEE Trans. Commun.*, vol. 68, no. 8, pp. 5028–5040, Aug. 2020.

[34] M. T. Mamaghani and Y. Hong, "Joint trajectory and power allocation design for secure artificial noise aided UAV communications," *IEEE Trans. Veh. Technol.*, vol. 70, no. 3, pp. 2850–2855, Mar. 2021.

[35] ——, "Intelligent trajectory design for secure full- duplex MIMO-UAV relaying against active eavesdroppers: A model-free reinforcement learning approach," *IEEE Access*, vol. 9, pp. 4447–4465, 2021.

[36] Y. Cai, Z. Wei, R. Li, D. W. K. Ng, and J. Yuan, "Joint trajectory and resource allocation design for energy-efficient secure UAV communication systems," *IEEE Trans. Commun.*, vol. 68, no. 7, pp. 4536–4553, Jul, 2020.

[37] X. Sun, C. Shen, T. Chang, and Z. Zhong, "Joint resource allocation and trajectory design for UAV-aided wireless physical layer security," in *Proc. IEEE GLOBALCOM Workshops*, Dec. 2018, pp. 1–6.

[38] T. Bai, J. Wang, Y. Ren, and L. Hanzo, "Energy-efficient computation offloading for secure UAV-edge-computing systems," *IEEE Trans. Veh. Technol.*, vol. 68, no. 6, pp. 6074–6087, Jun. 2019.

[39] M. Hua, Y. Wang, Q. Wu, H. Dai, Y. Huang, and L. Yang, "Energy-efficient cooperative secure transmission in multi-UAV-enabled wireless networks," *IEEE Trans. Veh. Technol.*, vol. 68, no. 8, pp. 7761–7775, Aug. 2019.

[40] C. Pan, H. Ren, Y. Deng, M. Elkashlan, and A. Nallanathan, "Joint blocklength and location optimization for URLLC-enabled uav relay systems," *IEEE Commun. Lett.*, vol. 23, no. 3, pp. 498–501, Mar. 2019.

[41] X. Lin, V. Yajnanarayana, S. D. Muruganathan, S. Gao, H. Asplund, H. Maattanen, M. Bergstrom, S. Euler, and Y. . E. Wang, "The sky is not the limit: LTE for unmanned aerial vehicles," *IEEE Commun. Mag.*, vol. 56, no. 4, pp. 204–210, Apr. 2018.

[42] W. Dinkelbach, "On nonlinear fractional programming," *Manage. Sci.*, vol. 13, no. 7, pp. 492–498, 1967.